


Article

Flexural Behavior of Beams Reinforced with FRP Bars: Test Database, Design Guideline Assessment, and Reliability Evaluation

Hau Tran ^{1,2,*} and Trung Nguyen-Thoi ^{3,4} ¹ Laboratory for Computational Civil Engineering, Institute for Computational Science and Artificial Intelligence, Van Lang University, Ho Chi Minh City 70000, Vietnam² Faculty of Civil Engineering, Van Lang School of Technology, Van Lang University, Ho Chi Minh City 70000, Vietnam³ Laboratory for Applied and Industrial Mathematics, Institute for Computational Science and Artificial Intelligence, Van Lang University, Ho Chi Minh City 70000, Vietnam; trung.nguyenthoi@vlu.edu.vn⁴ Faculty of Mechanical, Electrical, and Computer Engineering, Van Lang School of Technology, Van Lang University, Ho Chi Minh City 70000, Vietnam

* Correspondence: hau.tranquang@vlu.edu.vn

Abstract

The aims of this paper are to evaluate the current design procedures and to assess the reliability of FRP-reinforced concrete beams. Firstly, 299 FRP beams are collected to provide a useful source of data for other studies. The designs of these beams based on ACI 440.1R-15, CSA S806-02, and CEB-FIB are also summarized in detail. Secondly, a reliability analysis process considering the uncertainties of numerous variables of FRP-reinforced concrete beams is developed in Matlab R2024b. Based on this reliability analysis process, current prevalent design documents are rigorously assessed. Finally, the effect of numerous parameters on the reliability indices of FRP beams are investigated. The results of the study show that the developed procedure is highly reliable. Among three design documents, ACI 440.1R-15 can predict the ultimate moment of FRP-reinforced concrete beams better than others, as the mean and CoV of the model error are approximately 1.07 and 0.19, respectively. In addition, over 98% of beams designed by ACI 440.1R and CSA S806 meet the target reliability index. The design equations of CEB-FIB in the case of concrete crushing are less safe than those of ACI 440.1R and CSA S806.

Keywords: design guidelines; FRP-reinforced concrete beams; Monte Carlo method; reliability analysis; subset simulation



Academic Editor: Salvatore Verre

Received: 13 August 2025

Revised: 10 September 2025

Accepted: 11 September 2025

Published: 17 September 2025

Citation: Tran, H.; Nguyen-Thoi, T. Flexural Behavior of Beams Reinforced with FRP Bars: Test Database, Design Guideline Assessment, and Reliability Evaluation. *Buildings* **2025**, *15*, 3373. <https://doi.org/10.3390/buildings15183373>

Copyright: © 2025 by the authors. Licensee MDPI, Basel, Switzerland. This article is an open access article distributed under the terms and conditions of the Creative Commons Attribution (CC BY) license (<https://creativecommons.org/licenses/by/4.0/>).

1. Introduction

Steel-reinforced concrete members play a key role in the construction industry since they are crucial components of various kinds of structures, from residential houses to high-rise buildings or mega-dams [1,2]. Even though steel has numerous superior features that allow it to become a perfect partner of concrete, it can be attacked by chemicals and its structural durability will be reduced, especially in the case of marine structures. Under environmental factors such as chemical attacks or oxidation, steel bars can be deteriorated, leading to the load-carrying capacity of concrete structures declining [3]. These phenomena contribute to reducing the service life of structures and increasing maintenance costs. To cope with this problem, fiber-reinforced polymer (FRP) bars are utilized to replace traditional steel bars in concrete elements, since they have a lightweight nature, high tensile

strength, and a strong capability of chemical resistance [4–6]. However, fire can have certain influences on the behavior of FRP-reinforced concrete structures [7–9], which can limit the application of FRP as reinforcing bars.

Among FRP-reinforced concrete structures, FRP-reinforced concrete beams have drawn great attention from researchers with different kinds of studies on their behavior [10–19]. Notably, FRP bars used to reinforce concrete beams are manufactured mainly from basalt-fiber-reinforced polymer (BFRP) and glass-fiber-reinforced polymer (GFRP). The application of carbon-fiber-reinforced polymer (CFRP) bars as a type of reinforcement of concrete beams is quite limited due to their expensive cost. FRP is a brittle material with a linear stress–strain relationship, and the tensile strength and the elastic modulus of FRP bars (BFRP and GFRP) are in the range from 0.48 GPa to 4.9 GPa and 51.7 GPa to 110 GPa [4,20], respectively. In contrast, steel is a ductile material with an elastic–plastic stress–strain relationship and a much higher elastic modulus. Hence, the behavior and the failure mechanism of beams reinforced with steel and FRP are different. In addition, a comprehensive design process needs to be established for FRP-reinforced concrete beams, as they consist of two brittle materials (concrete and FRP bars). Currently, the design of FRP-reinforced concrete beams can be found in ACI 440.1R [21], CSA S806 [22], or CEB-FIB [23]. The common hypothesis of these design documents is that the section of the beam remains planar under loading conditions, sectional strain is linearly distributed, and the stress distribution of the concrete compression zone is converted to a rectangular stress block to simplify the calculation. Based on these assumptions and the equivalent equations, the loading capacity of the beam is determined, and this is multiplied with the reduction factors to find the allowable applied loads. There are two general forms indicated in the design documents [21–23] to check the safety of the designed structures, as follows:

$$\phi R_n(f_c, f_{fu}, \dots) \geq \sum \gamma_{Qi} Q_i \quad (1)$$

$$R_d(f_{ck}/\gamma_c, f_{fu}/\gamma_f, \dots) \geq \sum \gamma_{Qi} Q_i \quad (2)$$

The aforementioned design documents acknowledge that FRP-reinforced concrete beams should be designed to meet certain target reliability indices. Reliability indices reflect the failure probability of a structure. The higher the reliability index of a structure, the lower the failure probability of the structure and the safer that structure. In ACI 440.1R-15, the target reliability index is recommended to be 3.5, whilst the value of the target reliability index in CSA S806 and CEB-FIB can be taken as 3.8. Using the target reliability index and the reliability analysis, the resistance reduction factors and the partial safety factors can be evaluated. However, current studies on the reliability analysis and the assessment of prevalent design guidelines and standards of FRP-reinforced concrete beams are still limited. Hassanzadeh et al. [24] assessed ACI440.1R-15 using a first-order reliability method (FORM). Their study found that the provisions given by ACI for the design of FRP-reinforced concrete beams are quite conservative. They also proposed modified reduction factors for the design of these beams. Behnam and Eamon [25] conducted a reliability analysis based on the Monte Carlo method to optimize the design of FRP-reinforced concrete decks and beams. The purpose of their study was to minimize costs while making sure that the designed structures still met the safety requirements. He and Qiu [26] applied the Rackwitz–Fiessler method to carry out the reliability assessment of ACI 440.1R. Their study showed that the design using ACI 440.1R is conservative. They also proposed a new resistance reduction factor of 0.8 for the design of FRP-reinforced beams. Ribeiro and Diniz [27] calibrated the design recommendations given in ACI 440.1R based on the Monte Carlo method. Their study demonstrated that reliability indices of under-reinforced beams were higher than those in the transition zone and over-reinforced.

Although some studies have been conducted to evaluate the design guidelines of FRP reinforced concrete beams, there are still areas to be improved. Most of the previous studies only focus on ACI 440.1R and ignore other prevalent design guidelines and standards. Hence, studies on other design documents need to be carried out. In addition, a set of up-to-date tested specimens is necessary and useful for future studies on the flexural behavior of FRP-reinforced concrete beams, but such specimens are not fully available yet. Moreover, while the Monte Carlo method is a good reliability analysis approach and has been widely applied in many previous studies, it requires a large number of simulations and consumes lots of computational time. Therefore, a comprehensive study with an efficient reliability analysis procedure should be conducted to evaluate the reliability of FRP-reinforced concrete beams and to evaluate the current prevalent design documents. In this paper, a reliability analysis procedure based on subset simulation and the Monte Carlo method is developed in Matlab to assess the design guidelines and standards of FRP-reinforced concrete beams. It should be noted that this reliability analysis process only focuses on evaluating the ultimate flexural strength and the serviceability limit state is not considered. First, an up-to-date test database which includes 299 tested specimens has been collected to determine the model error of current design documents. These specimens can serve as a useful resource for future studies to calibrate their numerical models. Additionally, an extensive set of designed specimens is considered in the reliability analysis. Many key parameters are also investigated to explore their effects on the failure probability of FRP beams. Based on the results of the study, the design provisions of ACI 440.1R, CSA S806 and CEB-FIB are evaluated, and recommendations are provided.

2. Design of FRP RC Beams

In this section, three design documents including ACI 440.1R, CSA S806, and CEB-FIB are considered. To determine the flexural capacity of FRP-reinforced concrete beams, these design documents assume that the section of the beam remains plane under loading conditions, strain distributes linearly along the section, and the concrete compressive stress is converted to an equivalent rectangular stress block using reduction coefficients such as α_1 , β_1 , α_2 , β_2 , λ and η (see Figure 1). In the compression zone of the beam, FRP bars can be used to replace steel bars as steel bars can be corroded, which can lead to concrete cracking and spalling at this zone. FRP bars in the compression zone of the beams are not considered in the design equations and they do not affect the ultimate moment of FRP-reinforced concrete beams.

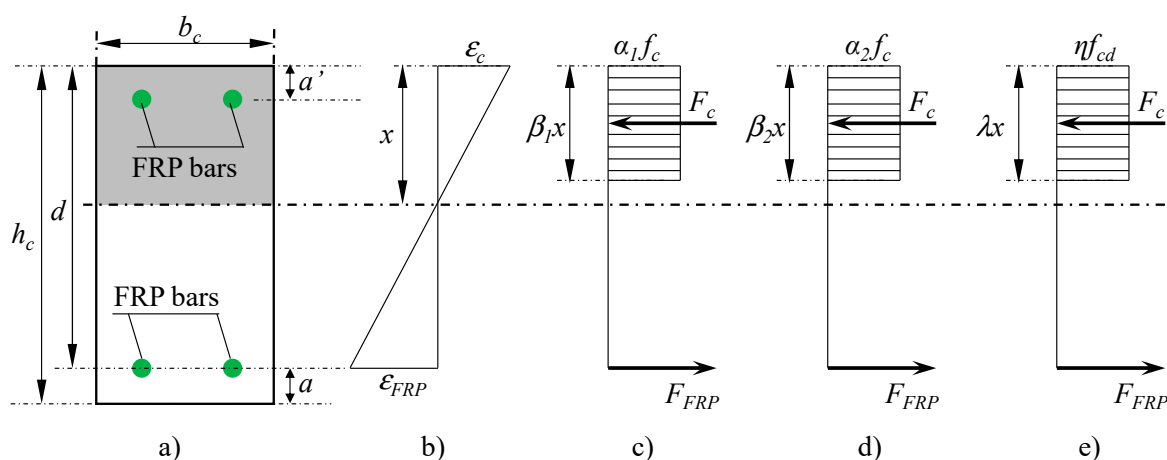


Figure 1. Distribution of strain and stress of rectangular sections: (a) section dimension; (b) strain distribution; (c) stress and forces of the section (ACI 440.1R); (d) stress and forces of the section (CSA S806); (e) stress and forces of the section (CEB-FIB).

2.1. ACI 440.1R-15

In ACI 440.1R, guidelines are provided for the design of FRP-reinforced concrete beams that fail by either FRP rupture or concrete crushing. To determine the type of failure mode in the design, the balanced FRP reinforcement ratio (ρ_{fb}) is compared with the FRP reinforcement ratio (ρ_f) of the section. These values are determined by Equations (3) and (4), respectively.

$$\rho_{fb} = \alpha_1 \beta_1 \frac{f_c}{f_{fu}} \frac{E_f \epsilon_{cu}}{E_f \epsilon_{cu} + f_{fu}} \quad (3)$$

$$\rho_f = \frac{A_f}{bd} \quad (4)$$

where α_1 and β_1 are the factors to convert the concrete compressive stress–strain diagram into an equivalent rectangular stress block, α_1 is taken as 0.85 and β_1 can be calculated by Equation (5).

$$\beta_1 = \begin{cases} 0.85 & \text{if } f_c \leq 28 \text{ MPa} \\ \max \left[\left(0.85 - 0.05 \times \frac{f_c - 28}{7} \right), 0.65 \right] & \text{if } f_c > 28 \text{ MPa} \end{cases} \quad (5)$$

In the case $\rho_f > \rho_{fb}$, the failure of the beam is dominated by concrete crushing. Based on the force equivalent equation and the strain compatibility, the nominal moment capacity of the beam can be determined by the following equations [21]:

$$M_n = A_f f_f \left(d - \frac{a}{2} \right) \quad (6)$$

$$a = \frac{A_f f_f}{0.85 f_c b} \quad (7)$$

$$f_f = E_f \epsilon_{cu} \frac{\beta_1 d - a}{a} \quad (8)$$

When $\rho_f < \rho_{fb}$, the beam will fail because of FRP rupture. In this case, the nominal moment capacity of the beam is determined by the equations as follows [21]:

$$M_n = A_f f_{fu} \left(d - \frac{\beta_1 c_b}{2} \right) \quad (9)$$

$$c_b = \left(\frac{\epsilon_{cu}}{\epsilon_{cu} + \epsilon_{fu}} \right) d \quad (10)$$

where a and c_b are the height of the concrete compression zone (mm). The design moment capacity is determined by multiplying the nominal moment capacity with a reduction factor that can be computed by Equation (11).

$$\phi = \begin{cases} 0.55 & \text{for } \rho_f \leq \rho_{fb} \\ 0.3 + 0.25 \frac{\rho_f}{\rho_{fb}} & \text{for } \rho_{fb} < \rho_f < 1.4 \rho_{fb} \\ 0.65 & \text{for } \rho_f \geq 1.4 \rho_{fb} \end{cases} \quad (11)$$

2.2. CEB-FIB

The concept for the design of FRP-reinforced concrete beams by CEB-FIB is relatively similar to that of ACI 440.1R as both concrete crushing and FRP rupture are considered. To

determine the type of failure mode, the reinforcement ratio of the section (ρ_f) is also compared with the balanced reinforcement ratio (ρ_{fb}) that is calculated by the equation below [23]:

$$\rho_{fb} = \frac{0.81(f_{ck} + 8)\varepsilon_{cu}}{f_{fk}\left(\frac{f_{fk}}{E_f} + \varepsilon_{cu}\right)} \quad (12)$$

When $\rho_f > \rho_{fb}$, the dominant failure mode of the beam is concrete crushing, and the moment capacity is calculated as follows [23]:

$$M_n = \eta f_{cd} b d^2 (\lambda \xi) \left(1 - \frac{\lambda \xi}{2}\right) \quad (13)$$

$$f_{cd} = \frac{f_{ck}}{\gamma_c} \quad (14)$$

$$\lambda = \begin{cases} 0.8 & \text{if } f_{ck} \leq 50 \text{ MPa} \\ 0.8 - \left(\frac{f_{ck}-50}{400}\right) & \text{if } 50 < f_{ck} \leq 90 \text{ MPa} \end{cases} \quad (15)$$

$$\eta = \begin{cases} 1.0 & \text{if } f_{ck} \leq 50 \text{ MPa} \\ 1.0 - \left(\frac{f_{ck}-50}{200}\right) & \text{if } 50 < f_{ck} \leq 90 \text{ MPa} \end{cases} \quad (16)$$

$$\xi = \frac{x}{d} = \frac{\varepsilon_{cu}}{\varepsilon_f + \varepsilon_{cu}} \quad (17)$$

$$\varepsilon_f = \frac{-\varepsilon_{cu} + \sqrt{\varepsilon_{cu}^2 + \frac{4\eta f_{ck} \lambda \varepsilon_{cu}}{\gamma_c \rho_f E_f}}}{2} \quad (18)$$

If $\rho_f < \rho_{fb}$, FRP rupture occurs, the moment capacity is determined by the following equation [23]:

$$M_n = \frac{A_f f_{fk} d}{\gamma_f} \left(1 - \frac{\xi}{2}\right) \quad (19)$$

$$\xi = \frac{x}{d} = \frac{\varepsilon_c}{\varepsilon_{fu} + \varepsilon_c} \quad (20)$$

To compute the height of the compression zone (x) and the concrete compressive strain at the top of the section (ε_c), equations based on the strain compatibility and force balance are established as follows:

$$\frac{\varepsilon_c}{\varepsilon_{fu}} = \frac{x}{d - x} \quad (21)$$

$$F_c = F_f \quad (22)$$

In CEB-FIB, F_c is calculated from the compressive stress by dividing the compression zone of the section into very small areas named as da (see Figure 2). The value of F_c is defined as follows:

$$F_c = \int_0^x f(\varepsilon) \cdot b \cdot da \quad (23)$$

where $f(\varepsilon)$ is the compressive stress of concrete (as shown in Figure 2). Based on the strain compatibility equation, the following equation can be established:

$$\frac{a}{d - x} = \frac{\varepsilon}{\varepsilon_{fu}} \quad (24)$$

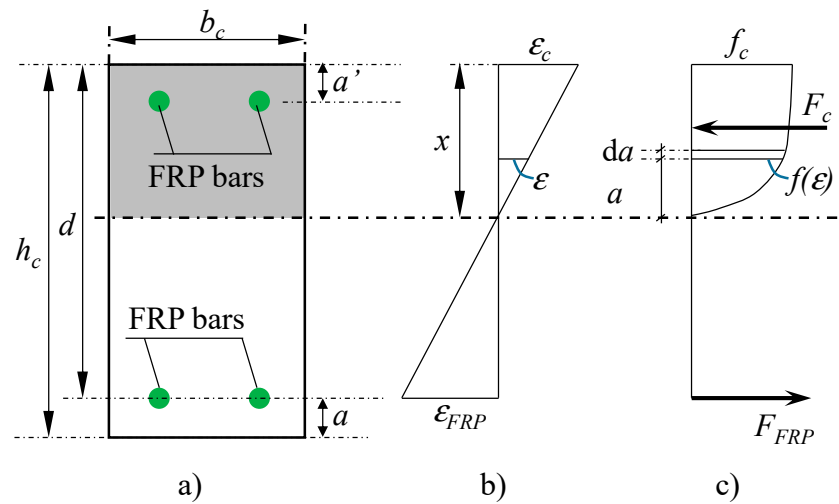


Figure 2. Calculation of F_c : (a) section dimension; (b) strain distribution; (c) stress distribution and forces.

From Equations (21) and (24), the values of a and its derivative can be determined as follows:

$$a = \frac{\epsilon \cdot x}{\epsilon_c} \quad (25)$$

$$da = \frac{x}{\epsilon_c} d\epsilon \quad (26)$$

If we substitute Equation (26) into Equation (23), F_c can be calculated as follows:

$$F_c = \int_0^{\epsilon_c} f(\epsilon) \cdot b \cdot \frac{x}{\epsilon_c} d\epsilon \quad (27)$$

In the case $\epsilon_{c2} < \epsilon_c \leq \epsilon_{cu}$, $f(\epsilon) = f_{cd}$ [28]. If we substitute this equation into Equation (27), the value of ϵ_c can be found as follows:

$$\epsilon_c = \frac{\epsilon_{fu} F_f}{f_{cd} b \cdot d - F_f} \quad (28)$$

$$F_f = \frac{A_f f_{fk}}{\gamma_f} \quad (29)$$

In the case $0 \leq \epsilon_c \leq \epsilon_{c2}$, $f(\epsilon) = f_{cd}(1 - (1 - \epsilon_c/\epsilon_{c2})^n)$ [28]. If we substitute this equation into Equation (27), the value of ϵ_c can be found by solving the following equation:

$$A \cdot \left(1 - \frac{\epsilon_c}{\epsilon_{c2}}\right)^{n+1} - A \cdot \left(1 - \frac{\epsilon_c}{\epsilon_{c2}}\right)^n + B \cdot \left(1 - \frac{\epsilon_c}{\epsilon_{c2}}\right) + C = 0 \quad (30)$$

where

n , ϵ_{c2} , and ϵ_{cu} are given in [28].

$$A = f_{cd} \cdot b \cdot d \cdot \epsilon_{c2} \quad (31)$$

$$B = \epsilon_{c2} F_f - A \quad (32)$$

$$C = A - (\epsilon_{c2} + \epsilon_{fu}) \cdot F_f \quad (33)$$

2.3. CSA S806-02

The failure mode in CSA can be detected by comparing the balanced reinforcement ratio (ρ_{fb}) with the reinforcement ratio (ρ_f). The value of ρ_{fb} is determined by Equation (34).

However, FRP rupture is not allowed in the design by CSA S806 [22]. As a result, the reinforcement ratio (ρ_f) of the designed FRP beam must be larger than the balanced reinforcement ratio (ρ_{fb}). In this case, the moment capacity of the designed beam is computed by Equation (35).

$$\rho_{fb} = \alpha_2 \beta_2 \frac{\phi_c f_c}{\phi_f f_{fu}} \frac{E_f \epsilon_{cu}}{E_f \epsilon_{cu} + f_{fu}} \quad (34)$$

$$M_n = \phi_f A_f f_f \left[d - \frac{a}{2} \right] \quad (35)$$

$$f_f = \left\{ \sqrt{\frac{(E_f \epsilon_{cu})^2}{4} + \frac{\phi_c \alpha_2 \beta_2 f_c}{\phi_f \rho_f} E_f \epsilon_{cu}} - \frac{E_f \epsilon_{cu}}{2} \right\} \leq f_{fu} \quad (36)$$

$$a = \frac{\phi_f A_f f_f}{\phi_c \alpha_2 f_c b} \quad (37)$$

where α_2 and β_2 are the factors used to convert concrete compressive stress to the equivalent rectangular stress block. These can be calculated by the following equations:

$$\alpha_2 = 0.85 - 0.0015 f_c \geq 0.67 \quad (38)$$

$$\beta_2 = 0.97 - 0.0025 f_c \geq 0.67 \quad (39)$$

3. Test Database

In this section, 299 simple supported beams reinforced with FRP bars have been collected from current studies [29–68]. The main criteria for selecting these beams include the type of failure (flexural failure), type of concrete, and type of FRP bars. The failure mode of these beams is flexural failure that includes concrete crushing or FRP rupture. Most of the collected beams are cast from normal or high strength Portland cement concrete, while several beams are cast from geo-polymer concrete and coral aggregate concrete. However, the type and strength of the concrete do not significantly affect the accuracy of the equations used to predict the ultimate moment of FRP-reinforced concrete beams. In the collected studies, GFRP, BFRP, AFRP, and CFRP are used to reinforce concrete beams. Among these types of FRP, GFRP is the most commonly used reinforcement as they are applied to reinforce almost 68.6% of the tested beams (around 205 beams). Beams reinforced by BFRP bars make up 15.7% with 47 beams. Beams reinforced by CFRP bars account for 11% with 33 beams. Beams reinforced with AFRP only account for approximately less than 4.7%. The type of FRP bars has certain influences on the accuracy of the equations used to predict the ultimate moment. Particularly, the ultimate moments of beams reinforced with GFRP, BFRP and AFRP predicted by the design equations (M_{pre}) agree quite well with experimental results (M_{test}) because the mean of M_{test}/M_{pre} is in the range from 0.98 to 1.11. In contrast, the mean of M_{test}/M_{pre} in the case of CFRP beams ranges from 1.15 to 1.3, which is slightly higher. This difference can be attributed to the higher modulus of CFRP. This parameter can affect the deformation, crack formation, crack propagation, and the height of the beam's compression zone, which leads to the influence on the ultimate moment of the beam. Due to the unique material properties of FRP, the flexural failure of FRP-reinforced concrete beams is relatively brittle and it includes two typical failure modes, concrete crushing and FRP rupture. Among the 299 collected specimens, 242 beams (approximately 81%) fail by concrete crushing, whilst 57 beams fail by FRP rupture. It shows that FRP rupture is not a desired failure mode since it is brittle, and it can lead to sudden damage. CSA S806 even does not allow FRP rupture to occur in the design [22].

The summary of the tested specimens is presented in Table 1, which includes the number of beams for each failure mode (number of specimens), and the range of basic parameters such as the width of the section (b_c), the height of the section (h_c), the compressive strength of concrete (f_c), the elastic modulus of FRP bars (E_f), and the ultimate tensile strength of FRP bars (f_{fu}). More details about the geometry and material properties of these beams can be found in Appendix A of the paper. Based on the test results of the collected beams, two typical failure modes, i.e., concrete crushing and FRP rupture, have been observed. In the case of FRP rupture, the failure is very brittle as it occurs suddenly without any clear warning due to the linear behavior of FRP. In contrast, the failure by concrete crushing is more ductile as cracks appear at the compression zone of the beam. Since the failure modes result in different stress and strain distributions in concrete and FRP, the calculation of the ultimate moment is also not similar. Therefore, in the current design documents, the calculation of ultimate moment is classified by the type of failure mode. According to ACI 440.1R [21] and CEB-FIB [23], the failure modes of FRP-reinforced concrete beams are classified by the reinforcement ratio (ρ_f), and the balanced reinforcement ratio (ρ_{fb}). Particularly, it is assumed in the design that concrete crushing occurs when $\rho_f > \rho_{fb}$, and FRP will rupture when $\rho_f \leq \rho_{fb}$. However, in practice, FRP rupture can also happen when $\rho_f > \rho_{fb}$. Therefore, ACI 440.1R recommends that the range from ρ_{fb} to $1.4\rho_{fb}$ is the transition zone, where either concrete crushing or FRP rupture can occur.

Table 1. Summary of the tested FRP-reinforced beams under bending forces.

		Number of Specimens	b_c (mm)	h_c (mm)	f_c (MPa)	E_f (GPa)	f_{fu} (MPa)
Concrete crushing	$\rho_f < \rho_{fb}$	6	150–200	250–450	47.7–114.9	41.6–49.64	620–896.3
	$\rho_f \geq \rho_{fb}$	236	80–500	120–400	20–97.4	35.63–148	551.58–2069
FRP rupture	$\rho_f < \rho_{fb}$	46	110–500	150–550	20–114.9	38–200	489.3–2000
	$\rho_f \geq \rho_{fb}$	11	100–280	175–380	20–105.2	40–148	520–2000

The distributions of parameters including the section dimensions and material properties are depicted in Figure 3. As can be seen from this figure, the collected beams cover both normal and high strength concrete, reinforced with either normal or high-strength FRP bars. Particularly, the values of b_c , h_c , f_c , E_f , and f_{fu} of the tested specimens fluctuate in a wide range from 80 mm to 500 mm, 120 mm to 550 mm, 20 MPa to 114.9 MPa, 35.6 GPa to 200 GPa, and 489.3 MPa to 2069 MPa, respectively. Among these specimens, 92% of the tested beams have a width from 100 mm to 250 mm, while 84% of the beams a height from 150 mm to 350 mm. Beams with concrete compressive strengths ranging from 25 MPa to 50 MPa account for 74%. In addition, 72% of the collected beams have an FRP modulus between 30 GPa and 60 GPa, while 73% of the beams have an FRP tensile strength from 600 MPa to 1200 MPa.

Based on the collected data and equations given in the considered design documents, M_{test}/M_{pre} ratios are determined. Subsequently, the Anderson–Darling goodness of fit test [69] is conducted to identify the distribution of the model error for each design guideline and standard. In this test, the p -value of each distribution is calculated. The type of distribution with the largest p -value, provided it exceeds 0.05, is chosen to represent the model error. Regarding ACI 440.1R, when the failure mode is concrete crushing, the values of mean and coefficient of variation (CoV) of the model error are 1.07 and 0.19, respectively. When FRP rupture is the dominant failure mode, the values of mean and CoV are 1.1 and 0.21, respectively. Based on the values of M_{test}/M_{pre} ratios, it has been found that Gumbel distribution (Figure 4) can reflect well the distribution of the model errors of both concrete

crushing and FRP rupture because the p -values obtained from Anderson–Darling test are larger than those of other distributions (see Table 2).

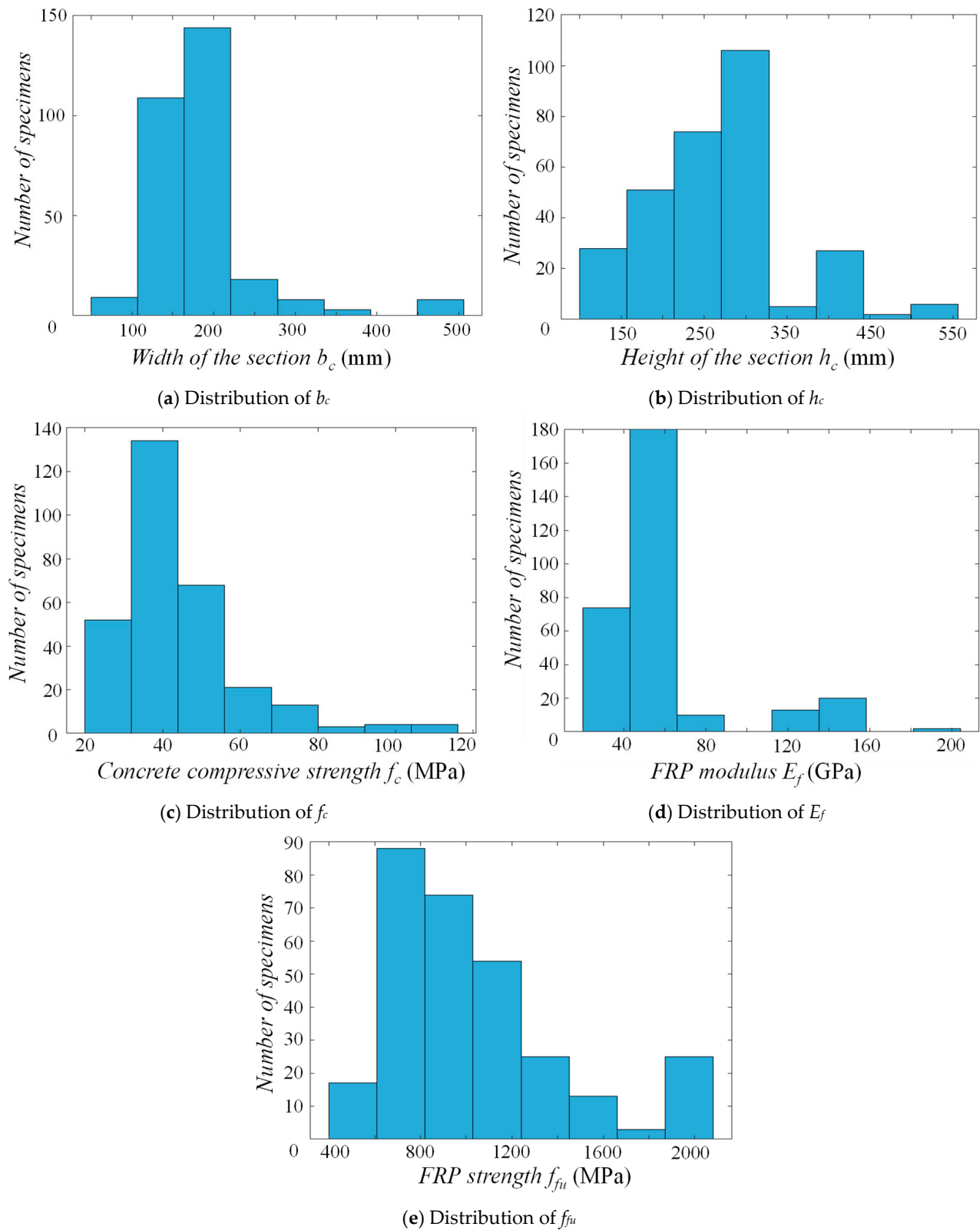


Figure 3. Key parameters of the collected FRP-reinforced concrete beams.

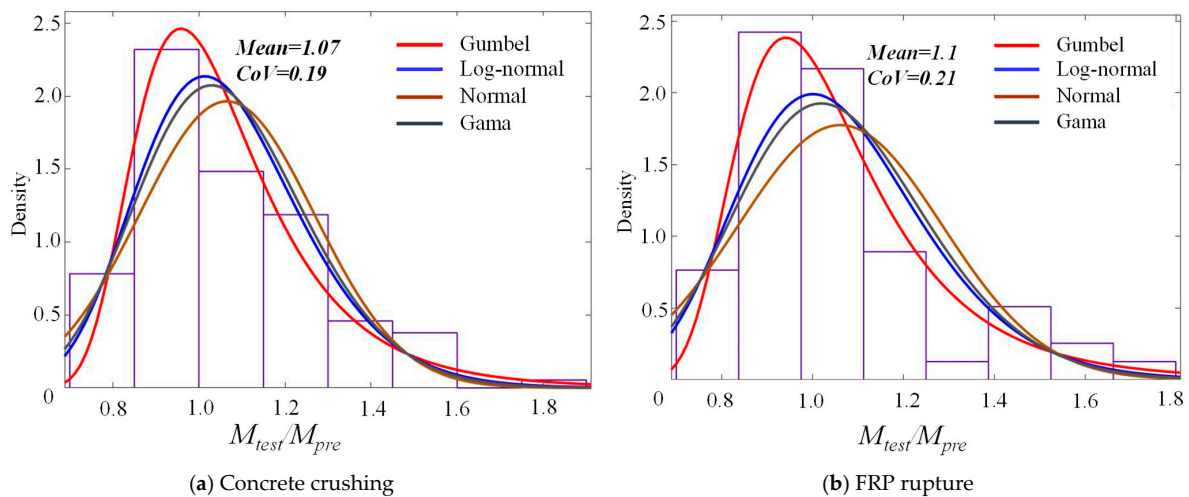


Figure 4. Model error for ACI 440.1R.

Table 2. p -value of the Anderson–Darling test.

Distribution	Concrete Crushing			FRP Rupture	
	ACI 440.1R	CEB-FIB	CSA S806	ACI 440.1R	CEB-FIB
Normal	1.5×10^{-7}	1.88×10^{-14}	2.6×10^{-6}	7.5×10^{-6}	0.00017
Lognormal	0.0052	0.0029	0.091	0.0038	0.018
Gamma	0.0046	0.0017	0.0205	0.0008	0.0054
Gumbel	0.0668	0.074	0.0003	0.11	0.072

In Figure 5, the influences of some basic parameters on the test-to-prediction moment ratios (M_{test}/M_{pre}) and the failure mode are depicted. As can be seen from this figure, ACI 440.1R obviously underestimates the moment capacity of FRP beams. Figure 5a demonstrates that ρ_f/ρ_{fb} can affect the type of failure mode significantly since the rise of this ratio can lead to the change in the failure mode of tested beams. When $\rho_f/\rho_{fb} < 1$, almost all the beams fail by FRP rupture, whilst most specimens fail by concrete crushing if $\rho_f/\rho_{fb} > 1.4$. When $1 < \rho_f/\rho_{fb} < 1.4$, either FRP rupture or concrete crushing can occur. As can be seen from Figure 5b, the section width-to-height ratio (b_c/h_c) also affects the values of M_{test}/M_{pre} and the type of failure mode. When this ratio rises, less fluctuation in the values of M_{test}/M_{pre} has been observed. When b_c/h_c is over 0.8, most of the collected beams fail by concrete crushing. Similarly, when FRP tensile strength increases over 1200 MPa, the failure mode of most of the collected beams is concrete crushing (Figure 5c). The fluctuation of concrete strength (f_c) also results in the variation of M_{test}/M_{pre} ratios, but they do not have significant influence on the failure modes as shown in Figure 5d.

Using the design provisions given by CEB-FIB, the failure mode and the ultimate moment are predicted. M_{test}/M_{pre} ratios are then calculated to determine the distribution of the model error. As can be seen from Table 2, Gumbel distribution provides the best fit for both concrete crushing and FRP rupture failure modes. The values of mean and CoV in the case of concrete crushing and FRP rupture are 1.15, 0.22 and 1.3, 0.2, respectively. More details about the distribution of the model error can be found in Figure 6. Figure 7 illustrates the effects of some principal parameters on the failure mode and the M_{test}/M_{pre} ratio. As can be seen from Figure 7a, the ρ_f/ρ_{fb} ratio can affect not only the M_{test}/M_{pre} ratio but also the type of failure mode. When ρ_f/ρ_{fb} rises, M_{test} and M_{pre} converge. When $\rho_f/\rho_{fb} < 1$, the main failure mode is FRP rupture, while $\rho_f/\rho_{fb} > 1$ leads to concrete crushing in almost all specimens. Figure 7b illustrates that when the section width-to-height ratio (b_c/h_c) increases, the M_{test}/M_{pre} ratio decreases. As shown in Figure 7c, the main failure

mode of the collected beams is concrete crushing when the tensile strength of FRP bar (f_{fu}) is larger than 1200 MPa. Figure 7d demonstrates that concrete compressive strength (f_c) does not significantly affect the failure mode or M_{test}/M_{pre} ratio.

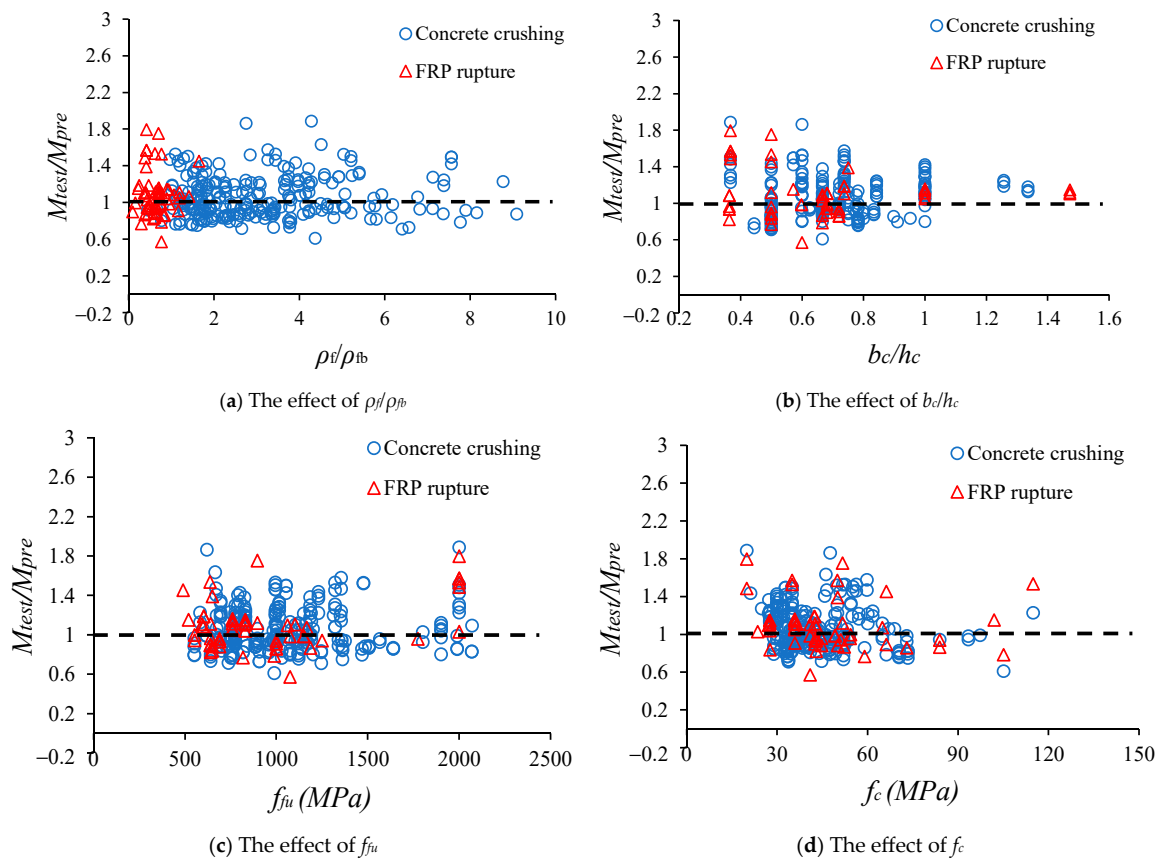


Figure 5. Effect of basic parameters on M_{test}/M_{pre} in the case of ACI.

The designed equations of CSA S806 are applied to determine the moment capacities of the collected beams. The comparison between the results calculated by CSA S806 and experimental results is depicted Figure 8. This figure shows that the formulas given in CSA S806 underestimate the moment capacities of the tested beams. Based on M_{test}/M_{pre} ratios, it has been found that the lognormal distribution (shown in Figure 9 and Table 2) with a mean of 1.13 and CoV of 0.21 can be the best fit for the model error in the case of CSA S806.

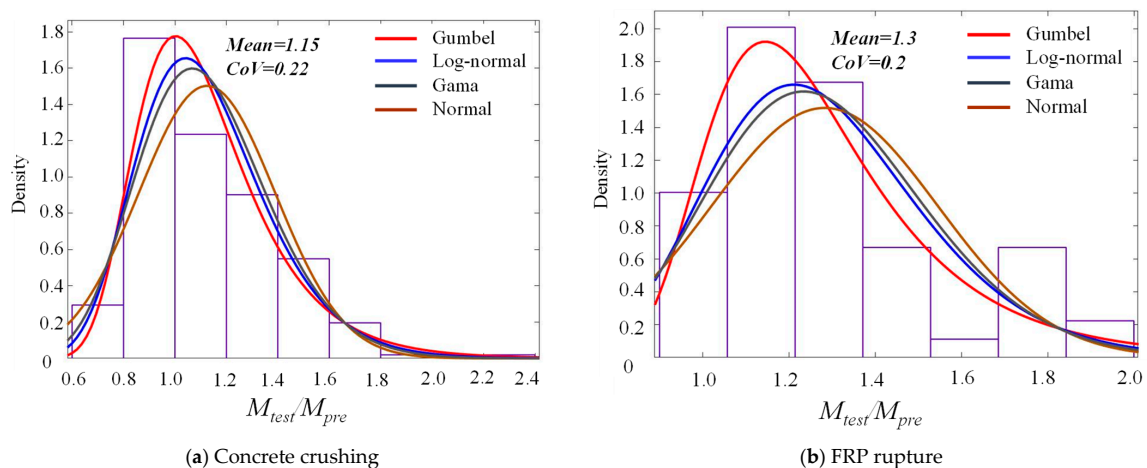


Figure 6. Model error for CEB-FIB.

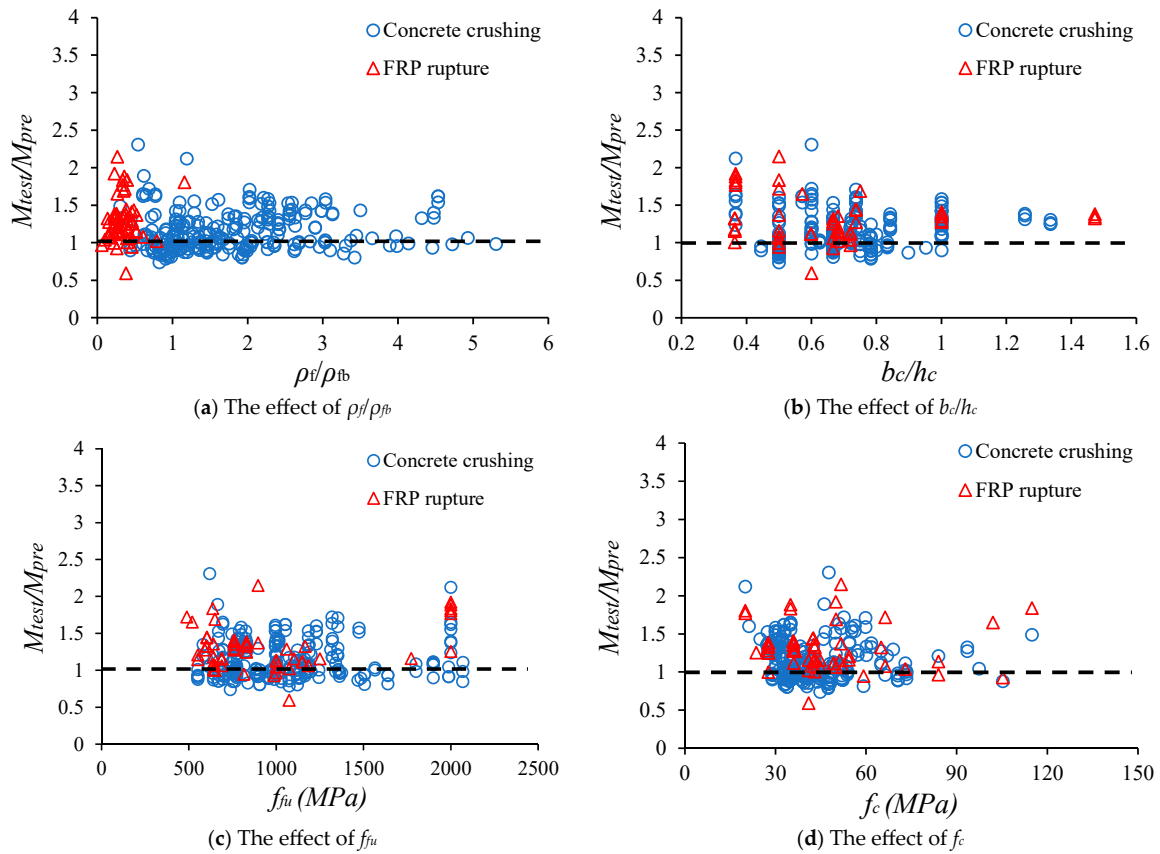


Figure 7. Effect of basic parameters on M_{test}/M_{pre} in the case of CEB-FIB.

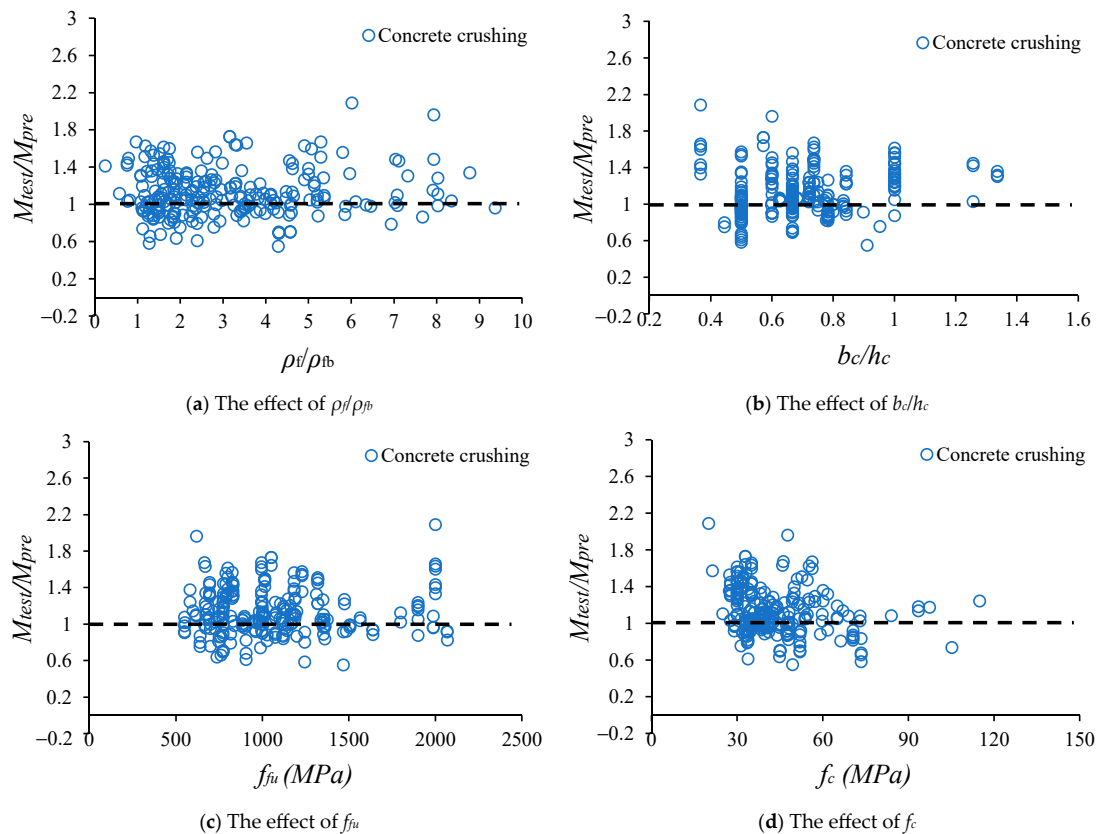


Figure 8. Effect of basic parameters on M_{test}/M_{pre} in the case of CSA S806.

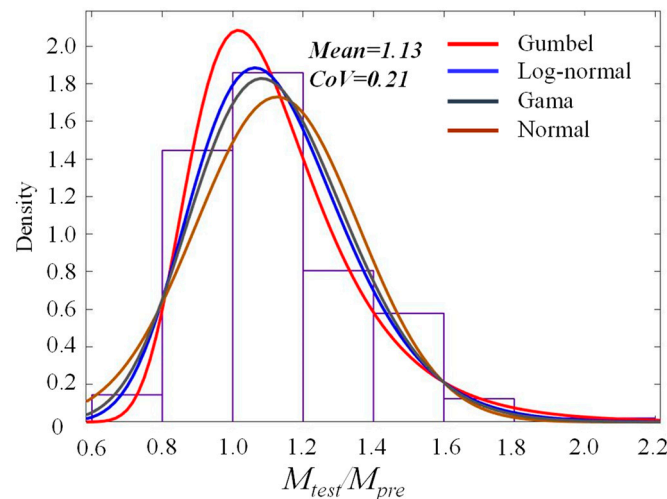


Figure 9. Model error for CSA S806.

4. Reliability Analysis of FRP-Reinforced Concrete Beams

In this section, reliability analysis is utilized to evaluate the failure probability and reliability index of FRP-reinforced concrete beams. Based on reliability indices, the safety of the designed beam can be evaluated and the reduction factor for the design can be calibrated. In this paper, an efficient and highly reliable procedure is developed to evaluate the reliability indices of beams designed by equations presented above.

4.1. Reliability Analysis Methods

Due to the uncertainty of variables such as concrete compressive strength, FRP bar tensile strength, the section width/height, or FRP bar area, the designed load-carrying capacity of FRP-reinforced concrete beams can differ from the predicted value. As a result, the designed beams can fail with a certain failure probability even when they are subjected to allowable loads. This failure probability is determined by reliability analysis, and it is defined by Equation (40) [70]. The reliability index is calculated based on failure probability by Equation (41) [71].

$$P_f = P_r[G(y_1, \dots, y_n) \leq 0] \quad (40)$$

$$\beta = -\Phi^{-1}(P_f) \quad (41)$$

where P_f is the probability of failure; P_r is the probability of the event in the bracket; $G(y)$ is the limit state function; y_1, \dots, y_n are the random variables such as applied loads, model errors, or material properties; Φ is the standard normal cumulative distribution function; Φ^{-1} is the inverse of the standard normal cumulative distribution function, which computes a value (in this case, it is the reliability index) corresponding to a particular probability. The limit state function plays a key role in the reliability analysis. Since this study only focuses on the strength limit state, the form of limit state function can be expressed as follows:

$$G(M) = ME \times M_R - M_L \quad (42)$$

where ME is the model error that accounts for the difference between the experimental results and the results obtained from the design equations as presented in Figures 4, 6 and 9.

Since the model error is dependent on the failure mode, the failure mode of each beam is determined by comparing the reinforcement ratio with the balanced reinforcement ratio calculated by each design document. After that, the model error for each failure mode will be applied in the reliability analysis procedure conducted by either Monte Carlo method or subset simulation. After obtaining the limit state function, Equation (40) can be solved

by several approaches to achieve the failure probability. In this paper, two methods that are Monte Carlo method [72] and subset simulation [73] are utilized. The details of Monte Carlo method are presented as follows:

- (a) At the beginning of the method, a set of N samples of the initial beams of the investigated beam is created using the statistical values of random variables given in Table 3.
- (b) For each generated sample, the failure mode is determined and the ultimate flexural moment (M_R) is calculated by the design equations. The moment caused by applied loads (M_L) is also computed.
- (c) Based on the values of these moments, the limit state function $G(M) = ME \times M_R - M_L$ (Equation (42)) is computed to determine whether the sample fails. It should be noted that a sample fails if the value of $G(M)$ is less than 0. Then, the number of failure samples can be calculated as follows: $N_f = N_f + 1$.
- (d) After all samples are analyzed, the value of P_f is defined as the ratio between the number of failure samples (N_f) and the initial N samples as given in Equation (43). The error of the result is calculated by Equation (44). More details of this calculation procedure are depicted in Figures 10 and 11.

$$P_f = \frac{N_f}{N} \quad (43)$$

$$Error = \sqrt{\frac{1 - P_f}{N \times P_f}} \quad (44)$$

Regarding subset simulation approach, the calculation procedure is presented as follows:

- (i) At the first step of the approach, the initial N samples of the investigated beam are generated by using their statistical values in Table 3.
- (ii) For each generated sample, the failure mode is determined and the ultimate flexural moment (M_R) is calculated by the design equations. The moment caused by applied loads (M_L) is also computed.
- (iii) In the third step, the values of $G(M) = ME \times M_R - M_L$ (Equation (42)) of all samples are calculated. The total number of failed samples N_f is counted if $G(M)$ is less than 0, and the failure probability of at the iteration number k -th is calculated as follows: $P_{f,k} = N_f/N$.
- (iv) In the next step, the p_o -percentiles of the values of $G(M)$ in step 3, namely c , are determined (p_o is taken as 0.1 [73]). Then, a set of samples whose $G(M)$ values are less than c will be extracted. This subset is used to generate new N samples and return to step 2.
- (v) Steps 2 to 4 are iterated until the value of c is less than 0. Then, the number of failure samples N_f of the last iteration is determined. The failure probability and the error are calculated by Equations (45) and (46), respectively. More details of this procedure are illustrated in Figures 12 and 13.

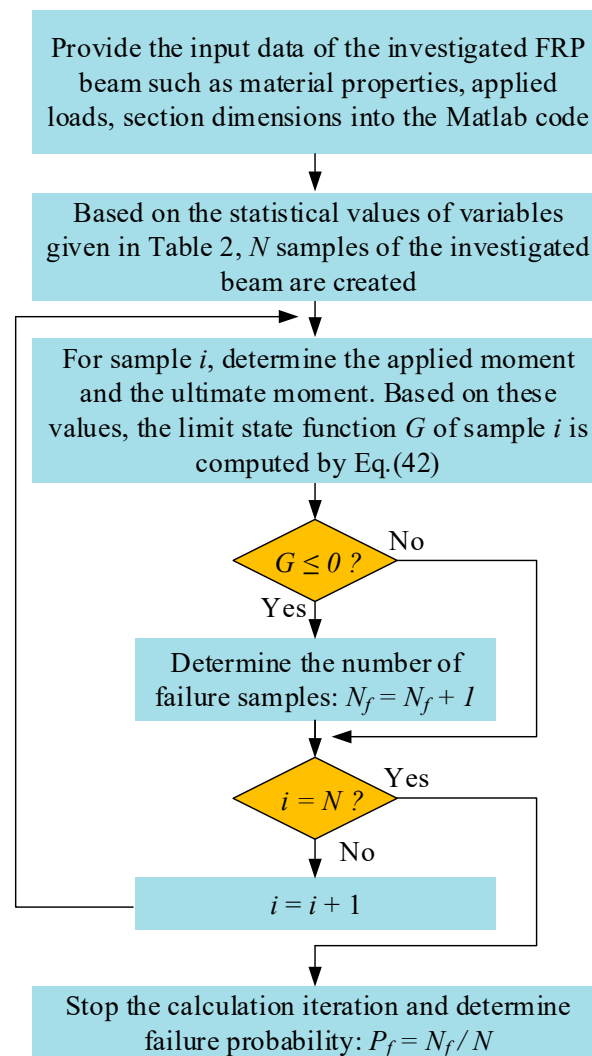
$$P_f = p_o^{n-1} \times \frac{N_f}{N} \quad (45)$$

$$Error = \sum_{k=1}^{n-1} \frac{1 - P_{f,k}}{N \times P_{f,k}} \gamma_k \quad (46)$$

where n is the total number of iterations, γ_k is the coefficient given in [73] and $P_{f,k}$ is the failure probability at iteration k -th.

Table 3. Statistical values of random variables.

Properties	Variables	Mean/Nominal Value	CoV	Ref.
Material	Elastic modulus of FRP, E_f	1.00	0.04	[74]
	FRP strength, f_{fu}	1.20	0.07	[75]
Geometry	Concrete compressive strength, f_c'	1.24	0.1	[24]
	Width of the concrete beam, b_c	1.00	0.02	[76]
	Height of the concrete beam, h_c	1.00	0.02	[76]
	FRP bar area, A_f	1.00	0.05	[75]
	Dead load, D_n (ACI)	1.05	0.10	[77]
	D_n (CSA, FIB)	1.00	0.05	[78]
	Live load, L_n (ACI)	1.00	0.25	[77]
	L_n (CSA, FIB)	0.60	0.35	[78]
Model error (ME)	ACI 440.1R:			
	Concrete crushing	1.07	0.19	
	FRP rupture	1.1	0.21	
	CEB-FIB:			
	Concrete crushing	1.15	0.22	
	FRP rupture	1.3	0.2	
	CSA S806:			
	Concrete crushing	1.13	0.21	

**Figure 10.** Procedure of Monte Carlo method.

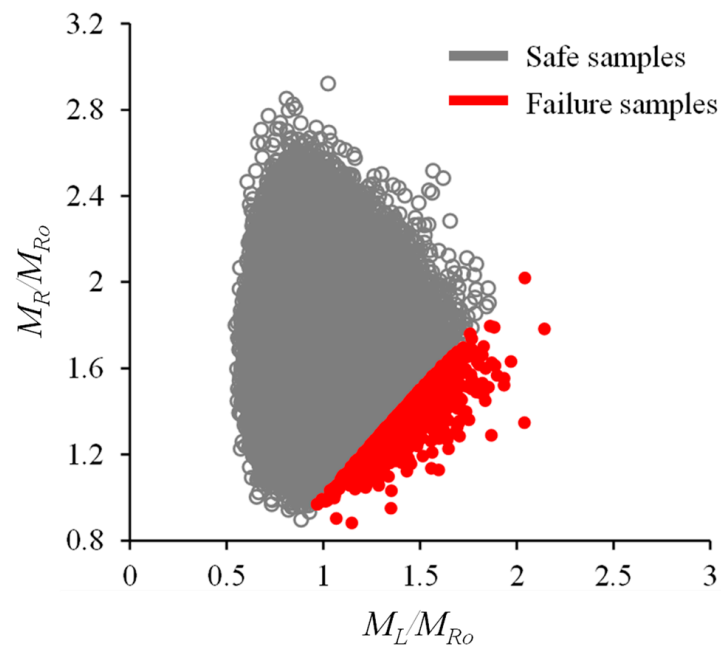


Figure 11. Relationship between M_R/M_{R0} and M_L/M_{R0} of beams generated by Monte Carlo method (M_{R0} is the ultimate moment of the investigated beam).

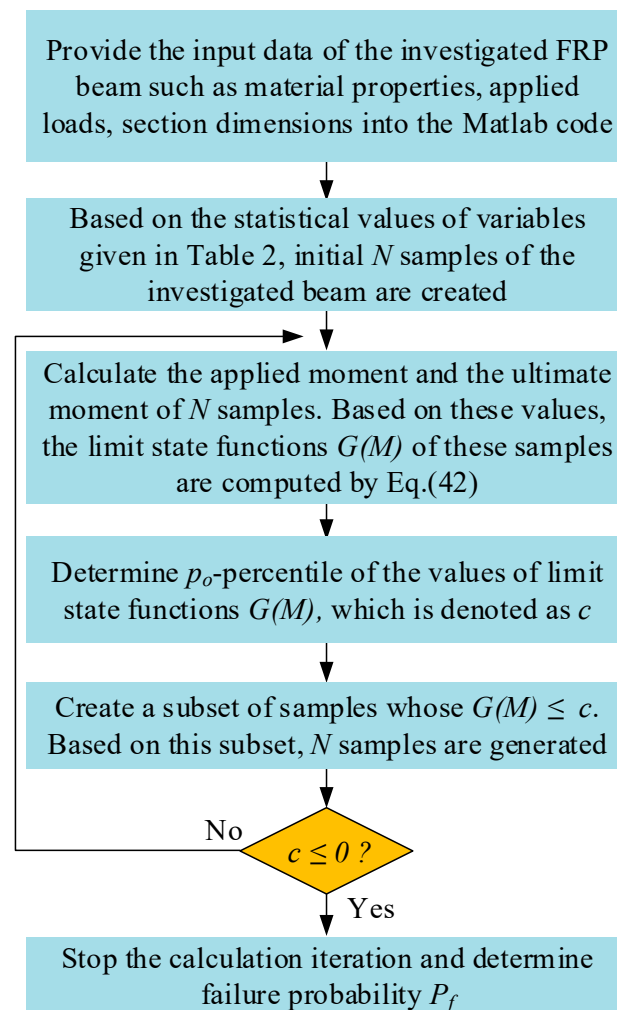


Figure 12. Subset simulation.

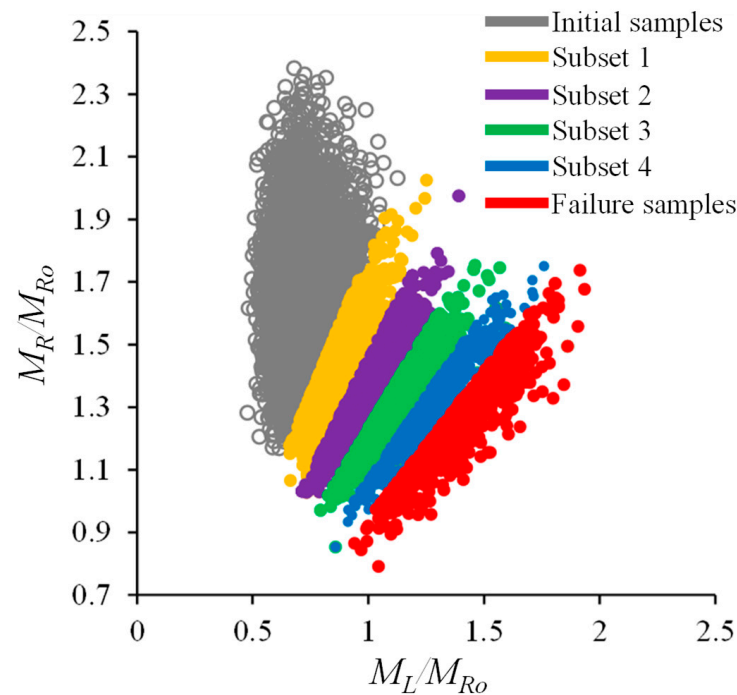


Figure 13. Relationship between M_R/M_{Ro} and M_L/M_{Ro} of beams generated by subset simulation.

The calculation processes of these two approaches are used to verify each other by conducting a reliability analysis of an FRP-reinforced concrete beam. This beam has a section width of 200 mm and a section height of 300 mm. The concrete compressive strength f_c , FRP tensile strength f_f and FRP elastic modulus E_f are 30 MPa, 483 MPa, and 50 GPa, respectively. The value of ρ_f / ρ_{fb} ratio fluctuates from 1.0 to 2.5. The uncertainty of variables, their mean-to-nominal ratios, CoV and type of distribution are presented in Table 3. The results of the reliability analysis are shown in Table 4, which demonstrates that the developed procedure is reliable since the reliability indices obtained from Monte Carlo method and subset simulation agree well with each other (the disparity is less than 5.0%). The number of samples are varied to investigate its influence on the reliability index. It can be seen from Table 5 that this parameter does not significantly affect the reliability index. However, to ensure an error of less than 10%, 5×10^6 samples are generated using the Monte Carlo method, while 7000 samples are used in the subset simulation.

Table 4. Comparison between Monte Carlo (MC) method and subset simulation.

β	ρ_f / ρ_{fb}				
	1.0	1.2	1.4	1.8	2.5
MC method	4.11	3.78	3.51	3.47	3.48
Subset simulation	4.12	3.88	3.59	3.48	3.42
Δ (%)	0.24	2.58	2.23	0.29	1.75

Table 5. The effect of number of samples on the reliability index.

N_{sample}	Monte Carlo							Subset Simulation					
	0.1×10^6	0.5×10^6	1×10^6	2×10^6	3×10^6	4×10^6	5×10^6	1×10^3	2×10^3	3×10^3	4×10^3	5×10^3	7×10^3
β	4.11	4.07	4.12	4.06	4.09	4.12	4.10	4.12	4.06	4.09	4.12	4.15	4.13

4.2. Designed Beams for the Reliability Analysis

To evaluate the presented design documents and investigate the effect of some basic parameters on the reliability indices of FRP-reinforced concrete beams, a group of beams is

designed. The compressive strength of concrete ranges from 20 MPa to 120 MPa. Particularly, $f_c = \{20, 50, 80, 100, 120\}$ MPa. The values of FRP tensile strength are $f_{fu} = \{483, 885, 1230, 1506, 1800, 2540\}$ MPa. The values of the modulus of FRP are $E_f = \{35, 50, 100, 150, 200\}$ GPa. The width of the section is $b_c = \{150, 200, 300, 400, 500\}$. The width-to-height ratio of the section is $b_c/h_c = \{0.25, 0.55, 0.85, 1.2, 1.5\}$. Another important parameter is the ρ_f/ρ_{fb} ratio, which is taken as $\rho_f/\rho_{fb} = \{0.2, 0.35, 0.5, 0.75, 0.95, 1.02, 1.5, 2.0, 2.5, 5.0\}$. In summary, the total number of specimens that will be used as the input for the reliability analysis is $5 \times 6 \times 5 \times 5 \times 5 \times 10 = 37,500$ specimens for each design guideline and standard. Regarding the applied loads, it is assumed that the nominal dead load D_n is equal to the nominal live load L_n throughout the study to conduct the analysis, and the effect of L_n/D_n ratio is only considered in the parametric study. It should be noted that other types of loads such as wind, snow, and earthquakes are not considered in this study. The load combinations in the case of combined D_n and L_n to determine the total applied load G are dependent on each design guideline and standard. Particularly, the load combinations are $G = 1.2D_n + 1.6L_n$, $G = 1.25D_n + 1.5L_n$, and $G = 1.35D_n + 1.5L_n$, corresponding to ACI, CSA, and CEB-FIB.

5. Results and Discussions

Based on the developed reliability analysis procedure, 37,500 FRP-reinforced concrete beams are analysed. The results of the analysis are presented in Figures 14 and 15, Tables 6 and 7. In Table 6, the range of the reliability indices is illustrated. In the case of concrete crushing, β is in the range from 3.02 to 5.06, 2.91 to 5.54, and 3.58 to 4.87 corresponding to ACI 440.1R, CEB-FIB, and CSA S806 standards. In the case of FRP rupture, β ranges from 3.48 to 5.01, and 3.21 to 5.23 corresponding to ACI 440.1R, and CEB-FIB model code. Figure 14 illustrates the range of reliability indices of the investigated beams. It should be noted in this figure that safe samples are beams with a reliability index higher than the target reliability index β_T , while failed samples have a reliability index smaller than β_T . As can be seen from the figure, the percentage of failed samples in the case of concrete crushing are higher than those in the case of FRP ruptures. Especially, there are no failed samples in the case of FRP rupture when beams are designed by ACI 440.1R (Figure 14a). The design by CSA S806 is also quite safe since very few beams fail (Figure 14e). Table 7 and Figure 15 present the percentage of specimens with the reliability indices exceeding the target reliability index β_T . In the case of ACI 440.1R, the percentage of specimens with a reliability index higher than β_T are 98.4% and 100% corresponding to concrete crushing and FRP rupture. In the case of the CEB-FIB model code, 95.6% of specimens exceed β_T when FRP rupture occurs. However, when the failure mode is concrete crushing, only approximately 81.3% of specimens exceed β_T . Hence, it is recommended to increase the safety factor for the design in this case. In the case of CSA, the percentage of specimens that have the reliability indices higher than β_T are 99.5%, which is quite high.

To investigate the influence of key parameters on the reliability indices of FRP-reinforced beams, a typical beam is selected. The width of the beam is 200 mm, the height of the beam is 300 mm, the compressive strength of concrete is 30 MPa, the tensile strength of FRP bars is 483 MPa, ρ_f/ρ_{fb} is 1.5 and the elastic modulus of FRP bars is 50 GPa.

Table 6. Reliability indices range of the investigated beams.

β	ACI 440	FIB	CSA
Concrete crushing	3.02–5.06	2.91–5.54	3.58–4.87
FRP rupture	3.48–5.01	3.21–5.23	-

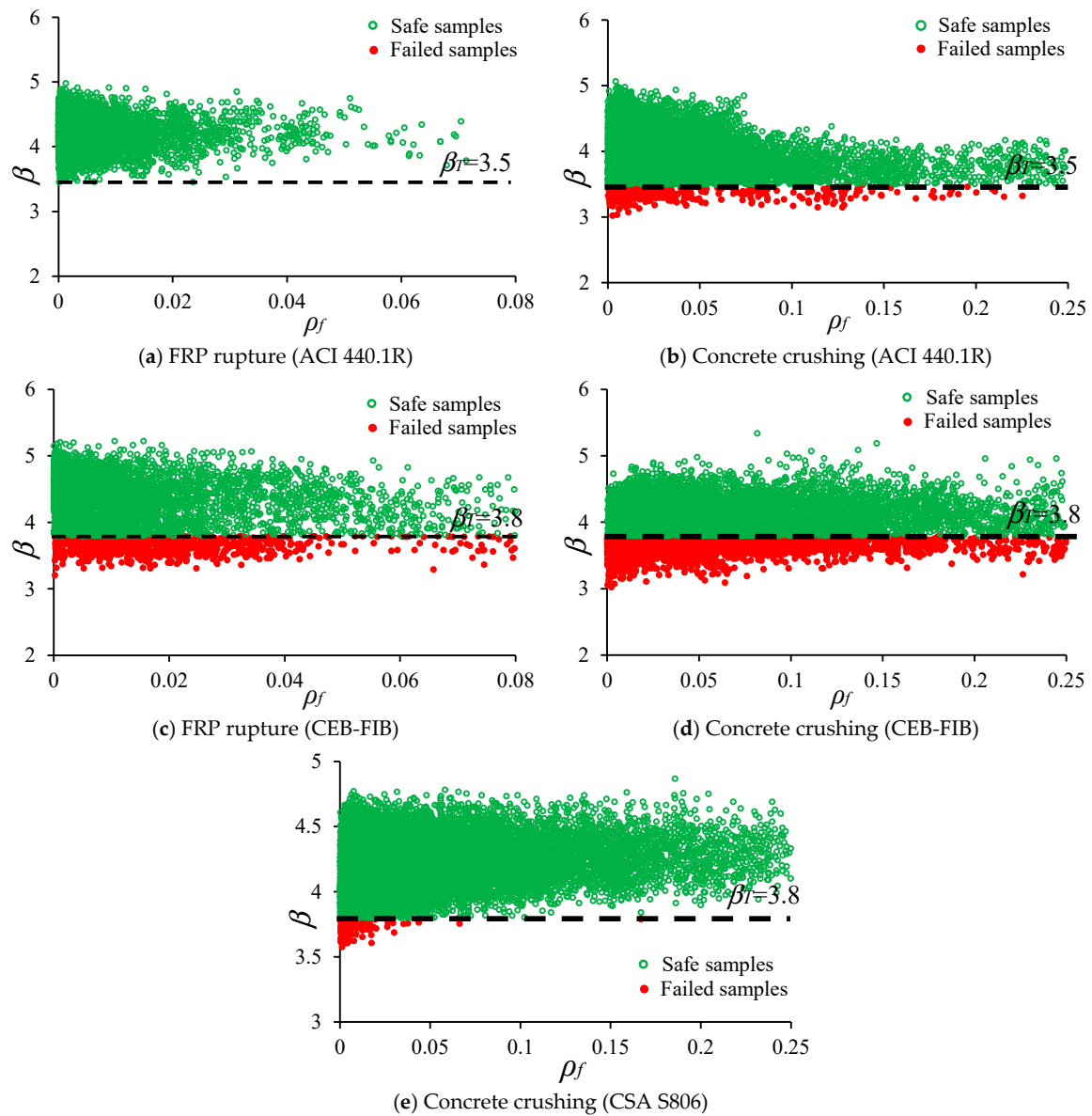


Figure 14. Reliability indices of the investigated beams determined by subset simulation.

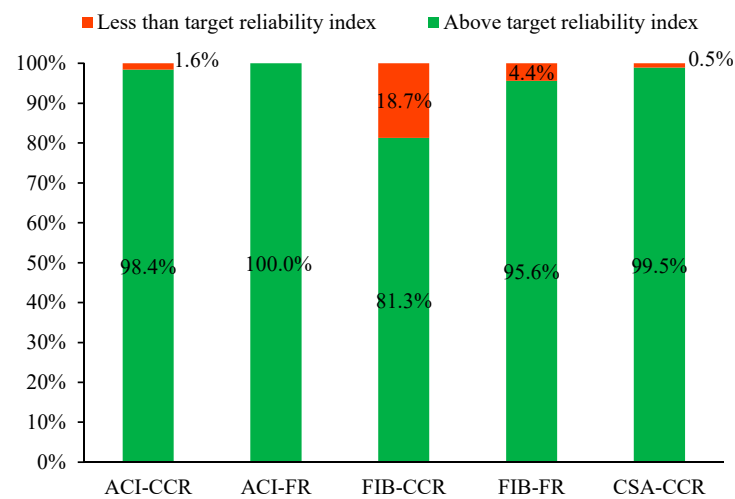


Figure 15. Percentage of specimens with reliability indices smaller/larger than the target reliability index.

Table 7. Percentage of beams corresponding to a specific range of reliability index.

Percentage of Specimen (%)	ACI		FIB		CSA	
	$\beta < 3.5$	$\beta \geq 3.5$	$\beta < 3.8$	$\beta \geq 3.8$	$\beta < 3.8$	$\beta \geq 3.8$
Concrete crushing	1.60	98.40	18.70	81.30	0.5	99.5
FRP rupture	0.00	100.00	4.40	95.60	-	-

5.1. The Effect of L_n/D_n Ratio

The influence of L_n/D_n ratio on the reliability indices of FRP-reinforced concrete beams is investigated by changing this ratio from 0.5 to 2.5. The specific values of L_n/D_n considered in this part are 0.5, 1.0, 1.5, 2.0, 2.5. The reliability indices β of beams corresponding to these ratios are determined by the proposed reliability analysis procedure, and the relationships between β and L_n/D_n are shown in Figure 16 and Table 8. Table 8 indicates that the reliability indices of beams designed by CSA S806 and CEB-FIB are obviously higher than those of beams designed by ACI 440.1R. This phenomenon occurs because the mean values of the live load given in CSA S860 and CEB-FIB are much smaller than that of ACI 440.1R (see Table 3). Moreover, Table 8 also reveals that the reliability indices go down when the L_n/D_n ratio rises. Figure 16 demonstrates the effects of L_n/D_n ratio and the model error (ME) on the reliability indices. In the case of ACI 440.1R, when the L_n/D_n ratio rises from 0.5 to 2.5, the values of the reliability indices diminish from 5.1 to 4.17, 3.75 to 3.395, and 4.61 to 4.02 corresponding to the simulation without model error, with model error ($CoV = 0.19$) and with $CoV = 0.1$. In the case of CSA S806, a similar trend to that of ACI440.1R has been observed. When the L_n/D_n ratio rises from 0.5 to 2.5, the values of the reliability indices reduce from 6.02 to 4.95, 4.22 to 3.91, and 5.8 to 4.75 corresponding to the simulation without model error, with model error ($CoV = 0.21$) and with $CoV = 0.1$. In the case of the CEB-FIB model code, the increase in L_n/D_n ratio from 0.5 to 2.5 also leads to a reduction in the reliability indices from 5.21 to 4.3, 4.09 to 3.81, and 4.97 to 4.05 corresponding to the simulation without model error, with model error ($CoV = 0.22$) and with $CoV = 0.1$. The reduction in the values of reliability index occurs because the CoV of the L_n (which is 0.25) is slightly larger than the CoV of the D_n (which is 0.1). As a result, when the value of L_n/D_n ratio grows, the failure probability increases, and the reliability index of the investigated beams decreases. In addition, it is obvious that the reliability indices decline significantly when the model error is applied (Figure 16).

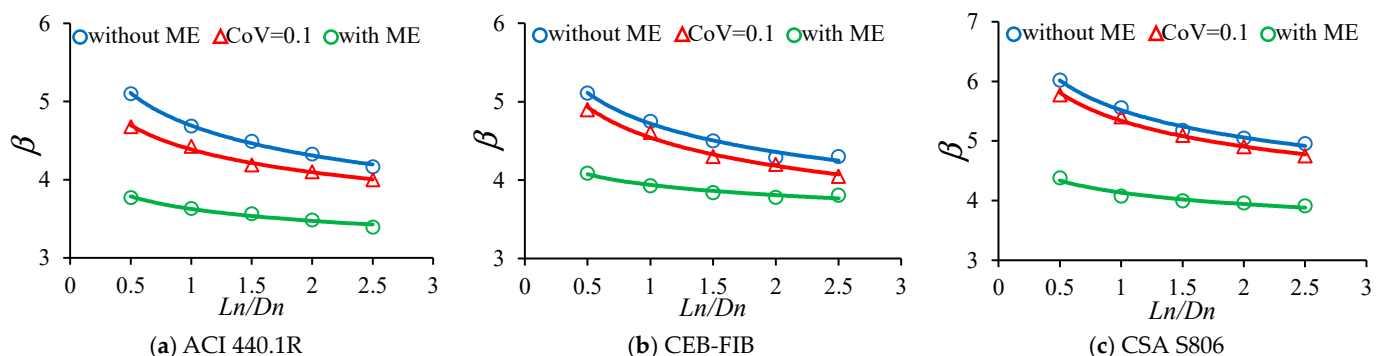
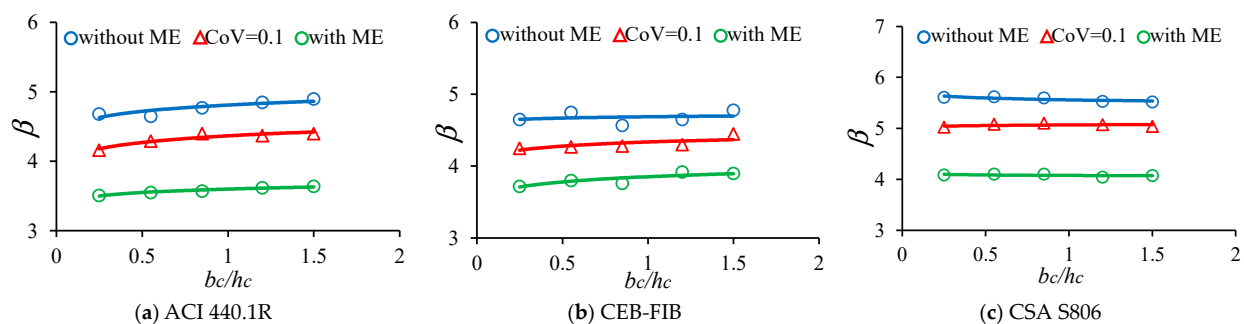
**Figure 16.** The effect of the L_n/D_n ratio on the reliability indices.

Table 8. The effect of L_n/D_n ratio on the reliability index of the investigated beam.

β	L_n/D_n				
	0.5	1.0	1.5	2	2.5
ACI 440.1R	3.751	3.632	3.566	3.483	3.395
CSA S806	4.216	4.072	3.993	3.957	3.910
CEB-FIB	4.09	3.930	3.840	3.780	3.810

5.2. The Effect of b_c/h_c Ratio

The influence of the b_c/h_c ratio on the reliability indices of the investigated FRP-reinforced concrete beams is illustrated in Figure 17 and Table 9. As can be seen from Table 9, the b_c/h_c ratio has a negligible effect on the reliability indices of the investigated beams. When b_c/h_c ratio is increased from 0.25 to 1.5, the reliability indices of beams designed by ACI 440.1R, CSA S806, and CEB-FIB fluctuate by approximately 3.7% (from 3.51 to 3.64), 0.27% (from 4.086 to 4.075), and 4.8% (from 3.72 to 3.9), respectively. More visible details are depicted in Figure 17. This figure also indicates that model error can affect the reliability indices of FRP-reinforced concrete beams significantly. When the model error is applied, the maximum reliability indices of the beams designed by ACI 440.1R, CSA S806 and CEB-FIB are 3.64, 4.1, and 3.92, respectively. However, when the model error is not considered, these values increase substantially to 4.91, 5.56, and 4.79 corresponding to significant increases of 34.9%, 35.6%, and 22.1%.

**Figure 17.** The effect of the b_c/h_c ratio on the reliability indices.**Table 9.** The effect of b_c/h_c ratio on the reliability index of the investigated beam.

β	b_c/h_c				
	0.25	0.55	0.85	1.2	1.5
ACI 440.1R	3.509	3.550	3.570	3.620	3.640
CSA S806	4.086	4.100	4.100	4.040	4.075
CEB-FIB	3.720	3.850	3.770	3.920	3.900

5.3. The Effect of ρ_f/ρ_{fb} Ratio

The ρ_f/ρ_{fb} ratio plays a critical role in the behavior of FRP-reinforced concrete beams. It also has certain influences on the reliability index of the beams as shown in Figure 18 and Table 10. In the case of the ACI design code (Figure 18a), the value of β almost remains constant when ρ_f/ρ_{fb} is less than 1.0. When ρ_f/ρ_{fb} increase from 0.95 to 1.5, β reduces gradually from 5.96 to 4.73, 5.54 to 4.56, 4.42 to 3.63 corresponding to the simulation without model error, with $CoV = 0.1$ and with model error. When ρ_f/ρ_{fb} exceeds 1.5, β almost remains constant. A notable observation is that when ρ_f/ρ_{fb} is larger than 1.0, the values of β in the case of ACI 440.1R decline gradually before it remains constant when ρ_f/ρ_{fb} is larger than 1.5. This phenomenon appears because the resistance of the beam is

reduced by a safety factor which increases from 0.55 to 0.65 when ρ_f/ρ_{fb} increases in this range (see Equation (11)). In the case of the CEB-FIB model code (Figure 18b), when ρ_f/ρ_{fb} rises from 0.75 to 1.02, β decreases significantly from 5.5 to 4.76, 5.1 to 4.57, 4.5 to 3.88 corresponding to the simulation without model error, with $\text{CoV} = 0.1$ and with model error. Once ρ_f/ρ_{fb} exceeds 1.0, the fluctuation in the value of β becomes negligible. In the case of CSA S806 (Figure 18c), the values of β vary slightly when ρ_f/ρ_{fb} is increased. It should be noted that FRP rupture is not permitted in the design by CSA; therefore, only $\rho_f/\rho_{fb} > 1.0$ is considered in the analysis.

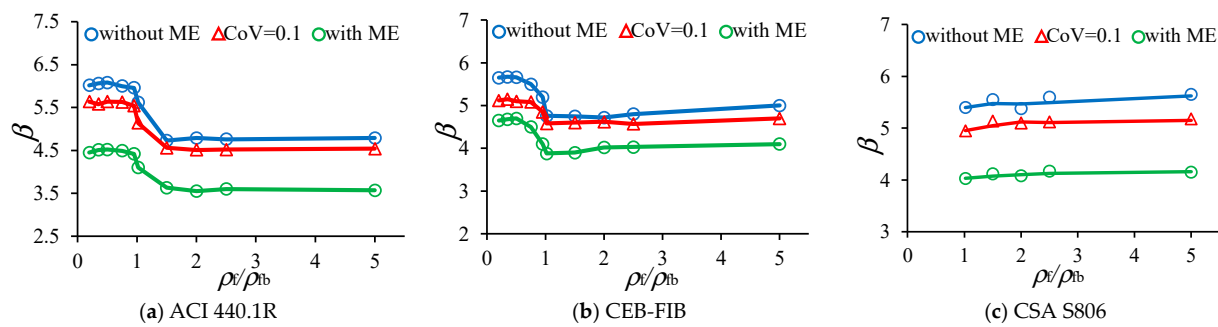


Figure 18. The effect of the ρ_f/ρ_{fb} ratio on the reliability indices.

Table 10. The effect of ρ_f/ρ_{fb} ratio on the reliability index of the investigated beam.

β	ρ_f/ρ_{fb}									
	0.2	0.35	0.5	0.75	0.95	1.02	1.5	2.0	2.5	5.0
ACI 440.1R	4.45	4.51	4.52	4.49	4.42	4.10	3.63	3.55	3.60	3.57
CSA S806	-	-	-	-	-	4.03	4.07	4.08	4.17	4.15
CEB-FIB	4.65	4.68	4.70	4.50	4.10	3.88	3.93	4.02	4.03	4.10

5.4. The Effect of f_{fu} and f_c

Figure 19 demonstrates that concrete compressive strength f_c has minimal influences on the reliability indices of the investigated beams. When f_c rises from 20 MPa to 120 MPa, the reliability indices of beams almost remain constant. In contrast, the model error affects the reliability indices dramatically. When the model error is accounted in the analysis, the maximum reliability indices of the beams designed by ACI 440.1R, CEB-FIB, and CSA S806 are 3.66, 3.97, and 4.13, respectively. However, when the model error is not considered, the maximum reliability indices of the beams increase significantly to 4.89, 4.72, and 5.58 corresponding to beams designed by ACI 440.1R, CEB-FIB, and CSA S806. Figure 20 illustrates that the effect of f_{fu} on the reliability indices of FRP-reinforced concrete beams is negligible.

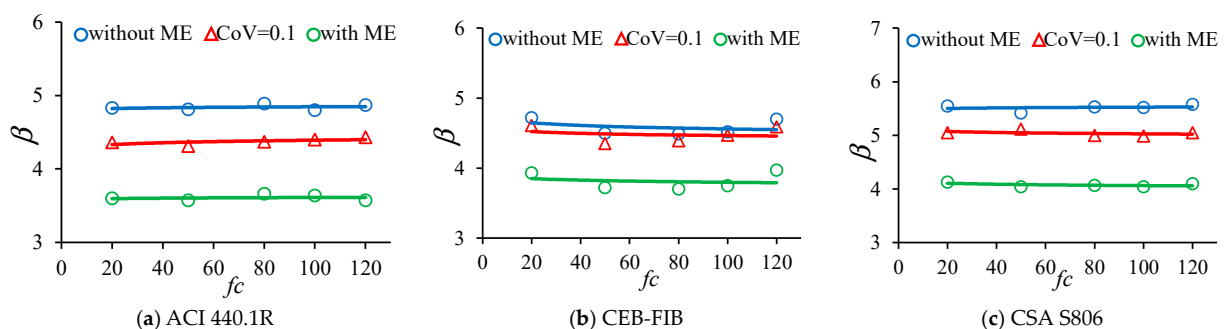


Figure 19. The effect of f_c on the reliability indices.

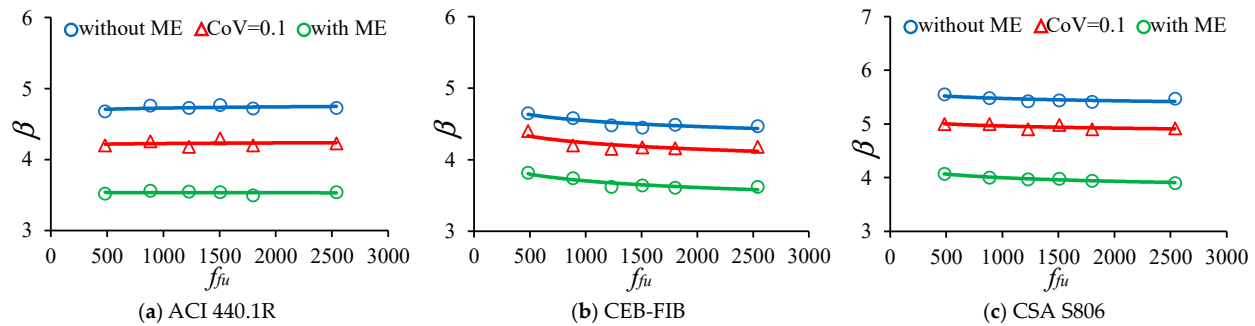


Figure 20. The effect of f_{fu} on the reliability indices.

6. Conclusions

This paper aims to develop an efficient reliability analysis procedure to evaluate the reliability of FRP-reinforced concrete beams designed by ACI 440.1R-15, CSA S806 and CEB-FIB. In the study, specimens tested in previous experimental studies are collected for the assessment. The design procedures of FRP beams based on ACI 440.1R, CSA S806 and CEB-FIB are reviewed and summarized in detail. In addition, source codes based on the Monte Carlo method and subset simulation are developed and the reliability analysis procedure of FRP beams is proposed. Based on the results of the study, some conclusions can be deduced as follows:

- (1) The geometry and material properties of 299 FRP-reinforced concrete beams have been collected and presented. This experimental data can be a useful resource for other studies related to FRP-reinforced concrete beams in the future.
- (2) All three design codes including ACI 440.1R, CSA S806 and CEB-FIB tend to underestimate the moment capacity of FRP-reinforced concrete beams. Among these three design guidelines, ACI 440.1R can predict the ultimate moment of FRP beams better than others because the mean and CoV of the model error in the case of concrete crushing are only 1.07 and 0.19, respectively, and those in the case of FRP rupture are 1.1 and 0.21, respectively.
- (3) Both three design documents can predict the ultimate moments of beams reinforced with GFRP and BFRP quite well. However, when beams are reinforced with CFRP, the ultimate moments determined by the design equations are relatively conservative. This discrepancy arises because the modulus of CFRP is quite higher than other types of FRP. It can affect the crack formation and stress distribution at the compression zone of concrete, which can affect the ultimate moment. This effect can be considered to improve the design equations.
- (4) The developed source code and the proposed reliability analysis procedure are reliable as the difference between results of the Monte Carlo method and subset simulation is less than 5%. Based on the results of the reliability analysis, it has been found that ACI 440.1R and CSA S806 can be applied to design FRP beams effectively as more than 98% of the specimens designed by these standards meet the target reliability index. However, the design equations of CEB-FIB for the case of concrete crushing are less safe than those of ACI 440.1R and CSA S806 since approximately 18% of the specimens have reliability indices smaller than the target reliability index. These discrepancies can be attributed to the differences in the model error, load factors, target reliability indices and resistance factors of each design document.
- (5) The reduction factor given in ACI 440.1R to determine the design moment of beams failed by FRP rupture is quite conservative. Further studies can be conducted to calibrate and increase this parameter.

- (6) The parametric study illustrates that model error, live load-to-dead load ratio (L_n/D_n) and reinforcement-to-balanced reinforcement ratio (ρ_f/ρ_{fb}) have significant influences on the reliability indices of the FRP-reinforced concrete beams. In contrast, variations in the fabrication, material and geometric parameters have negligible influence on the reliability results.

Author Contributions: Conceptualization, H.T. and T.N.-T.; methodology, H.T.; software, H.T.; validation, H.T.; formal analysis, H.T.; investigation, H.T.; resources, H.T., and T.N.-T.; data curation, H.T.; writing—original draft preparation, H.T.; writing—review and editing, H.T., and T.N.-T.; visualization, H.T., and T.N.-T.; supervision, T.N.-T.; project administration, H.T., and T.N.-T. All authors have read and agreed to the published version of the manuscript.

Funding: This research received no external funding.

Institutional Review Board Statement: Not applicable.

Data Availability Statement: Data will be made available upon reasonable request.

Conflicts of Interest: The authors declare no conflicts of interest.

Abbreviations

The following abbreviations are used in this manuscript:

A_f	area of FRP bars (mm^2)
b_c	width of the beam section (mm)
d	effective depth of the section (mm)
E_f	elastic modulus of FRP bars (MPa)
f_{fu}	ultimate tensile strength of FRP (MPa)
f_{fk}	characteristic tensile strength of FRP (MPa)
f_f	tensile stress of FRP bars (MPa)
f_c	compressive strength of concrete (MPa)
f_{ck}	characteristic compressive strength of concrete (MPa)
f_{cd}	design value of concrete compressive strength (MPa)
$G(M)$	limit state function
h_c	height of the beam section (mm)
ME	model error
M_L	moment caused by applied loads (kNm)
M_n	nominal moment capacity of the beam (kNm)
M_{pre}	moment of the beam predicted by design equations (kNm)
M_R	ultimate flexural moment (kNm)
M_{test}	moment of the beam obtained from experiment (kNm)
N	number of samples generated in the reliability analysis
N_f	number of failure samples in the reliability analysis
P_f	failure probability
Q_i	applied loads (kN)
R_d	design resistance of the beam (kNm)
R_n	nominal load—carrying capacity of the investigated beam (kNm)
x	distance from extreme compression fiber to neutral axis (mm)
β	reliability index
γ_c, γ_f	partial safety factors of concrete and FRP
γ_{Qi}	load factors
ϵ_{cu}	ultimate compressive strain of concrete
ϵ_f	strain of FRP bar
ϵ_c	compressive strain of concrete
ρ_f	reinforcement ratio of the beam section

ρ_{fb}	reinforcement ratio of the beam section
ϕ	reduction factor of the nominal load-carrying capacity
ϕ_c	resistance factor for concrete
ϕ_f	resistance factor for FRP

Appendix A

Table A1. Tested specimens.

Specimen	b_c (mm)	h_c (mm)	f_c (MPa)	A_f (mm ²)	E_f (GPa)	f_f (MPa)	M_{exp} (kNm)	Failure	Ref.
COMP-00	200	240	35.3	508.1	43.37	885	41.37	CR	[33]
COMP-25	200	240	35.3	508.1	43.37	885	39.06	CR	
COMP-50	200	240	36.4	508.1	43.37	885	39.35	CR	
COMP-75	200	240	36.4	508.1	43.37	885	40.60	CR	
BC2HA	130	180	57.2	237.7	38.00	773	19.70	CR	[66]
BC2HB	130	180	57.2	237.7	38.00	773	20.60	CR	
BC4NB	130	180	46.2	475.3	38.00	773	20.60	CR	
BC4HA	130	180	53.9	475.3	38.00	773	21.00	CR	
BC4HB	130	180	53.9	475.3	38.00	773	21.40	CR	
BC4VA	130	180	93.5	475.3	38.00	773	28.40	CR	
BC4VB	130	180	93.5	475.3	38.00	773	29.50	CR	
BC2VA	130	180	97.4	237.7	38.00	773	22.70	CR	
GB3-1	180	300	35.0	506.7	40.00	695	71.00	CR	[52]
GB3-2	180	300	35.0	506.7	40.00	695	70.50	CR	
GB1-1	180	300	35.0	253.4	40.00	695	60.00	CR	
GB1-2	180	300	35.0	253.4	40.00	695	59.00	CR	
GB2-1	180	300	35.0	380.0	40.00	695	65.00	CR	
GB2-2	180	300	35.0	380.0	40.00	695	64.30	CR	
C1-6	200	300	39.3	425.3	114.00	1506	83.13	CR	
C1-8	200	300	39.3	567.1	114.00	1506	90.39	CR	
C2-4	200	300	39.9	254.5	122.00	1988	78.75	CR	[54]
C2-6	200	300	40.8	381.7	122.00	1988	80.89	CR	
C2-8	200	300	40.8	508.9	122.00	1988	89.39	CR	
G1-6	200	300	39.1	760.1	40.00	617	77.47	CR	
G1-8	200	300	39.1	1013.4	40.00	617	86.76	CR	
G2-6	200	300	39.1	678.6	36.00	747	71.00	CR	
G2-8	200	300	39.1	904.8	36.00	747	84.54	CR	
AR-6	200	300	39.1	425.3	52.00	1800	70.85	CR	
AR-8	200	300	39.1	567.1	52.00	1800	71.75	CR	
C1-4	200	300	40.4	283.5	114.00	1506	71.20	CR	
4FRP1	203	152	27.6	320.0	41.40	830	15.78	CR	
4FRP2	203	152	27.6	320.0	41.40	830	15.58	CR	[79]
4FRP3	203	152	27.6	320.0	41.40	830	16.29	CR	
5FRP1	191	152	27.6	320.0	41.40	830	16.37	CR	
5FRP2	191	152	27.6	320.0	41.40	830	16.65	CR	
5FRP3	191	152	27.6	320.0	41.40	830	15.78	CR	
1FRP1	381	203	27.6	80.0	41.40	830	11.49	FR	
1FRP2	381	203	27.6	80.0	41.40	830	12.67	FR	
1FRP3	381	203	27.6	80.0	41.40	830	11.49	FR	
2FRP1	318	216	27.6	80.0	41.40	830	13.62	FR	
2FRP2	318	216	27.6	80.0	41.40	830	13.26	FR	
2FRP3	318	216	27.6	80.0	41.40	830	13.06	FR	
CB3B-1	200	300	52.0	523.1	37.60	773	66.00	CR	
CB3B-2	200	300	52.0	523.1	37.60	773	64.80	CR	
CB4B-1	200	300	45.0	697.5	37.60	773	75.40	CR	[80]
CB4B-2	200	300	45.0	697.5	37.60	773	71.70	CR	
CB6B-1	200	300	45.0	1046.2	37.60	773	84.80	CR	

Table A1. Cont.

Specimen	b_c (mm)	h_c (mm)	f_c (MPa)	A_f (mm ²)	E_f (GPa)	f_f (MPa)	M_{exp} (kNm)	Failure	Ref.
CB6B-2	200	300	45.0	1046.2	37.60	773	85.40	CR	
CB2B-1	200	300	52.0	348.7	37.60	773	57.90	CR	
CB2B-2	200	300	52.0	348.7	37.60	773	59.80	CR	
GB5	150	250	25.0	429.4	45.00	1000	40.30	CR	[44]
GB9	150	250	31.8	429.4	45.00	1000	39.73	CR	
GB10	150	250	31.8	429.4	45.00	1000	39.50	CR	
II	200	210	31.3	1134.1	35.63	700	34.19	CR	[34]
III	200	260	31.3	506.7	43.37	886	45.13	CR	
IV	200	300	40.7	567.1	35.63	700	59.19	CR	
V	200	250	40.7	1134.1	35.63	700	57.00	CR	
B7	152.4	152.4	49.3	99.0	140.00	1900	17.10	CR	[67]
B8	152.4	152.4	51.1	99.0	140.00	1900	16.92	CR	
B9	152.4	152.4	53.3	99.0	140.00	1900	16.58	CR	
B12	152.4	152.4	43.9	142.4	140.00	1900	17.51	CR	
B4	152.4	152.4	51.7	63.3	140.00	1900	12.60	CR	
B5	152.4	152.4	48.0	63.3	140.00	1900	10.15	CR	
N2#13G2	200	400	33.5	261.2	67.00	1639	82.78	CR	[46]
N5#15G2	200	400	29.0	970.4	69.30	1362	129.32	CR	
N6#15G1	200	400	33.5	1161.9	50.00	762	118.73	CR	
H5#15G2	200	400	73.4	970.4	69.30	1362	178.00	CR	
N5#15G3	200	400	33.8	970.4	59.50	1245	110.58	CR	
H6#15G1	200	400	73.4	1161.9	50.00	762	177.73	CR	
N2#25G3	200	400	33.8	1019.3	60.30	906	115.93	CR	
H5#15G3	200	400	73.4	1040.0	59.50	1245	188.37	CR	
H2#25G3	200	400	73.4	1019.3	60.30	906	189.06	CR	
N3#13G1	200	400	33.5	384.9	48.70	817	81.34	CR	
H2#13G2	200	400	59.1	261.2	67.00	1639	101.59	CR	
H3#13G1	200	400	59.1	384.9	48.70	817	85.58	FR	
C4	152.4	304.8	29.0	1012.9	45.50	551.58	54.24	CR	[49]
C8	152.4	304.8	34.5	774.2	50.60	551.58	56.45	CR	
C-H5	152.4	304.8	44.8	1006.5	45.50	551.58	74.24	CR	
CC	152.4	304.8	44.8	1006.5	45.50	551.58	81.36	CR	
EH4	152.4	304.8	44.8	354.8	47.70	896.32	50.85	CR	
EH2	152.4	304.8	44.8	380.6	48.30	737.74	42.21	CR	
P4G	178	229	48.0	219.0	124.00	2069	51.00	CR	[63]
P8G	178	229	48.0	723.0	41.00	690	47.00	CR	
P4C	178	229	48.0	1077.0	41.00	552	51.00	CR	
G2.1-A90	280	380	41.3	1963.5	38.00	582	237.93	CR	[57]
G2.1-A135	280	380	33.9	1963.5	38.00	582	236.78	CR	
G0.4-A135	280	380	42.3	339.3	40.20	603	80.40	FR	
G0.5-A135	280	380	42.5	452.4	40.20	603	107.30	FR	
G0.8-A90	280	380	36.6	804.2	40.00	593	158.80	FR	
S-C-O	500	150	53.7	565.5	137.00	1375	57.50	CR	[81]
S-C-U	500	150	54.3	150.8	137.00	1773	29.50	FR	
S-B-O	500	150	55.0	392.7	50.00	1350	42.40	CR	[58]
S-B-U	500	150	51.2	150.8	50.00	1250	21.00	FR	
G30W-A	150	300	21.3	226.9	52.00	1230	47.30	CR	[51]
G30W-B	150	300	27.3	314.0	52.00	1230	59.60	CR	
G40W-A	150	300	27.2	226.9	52.00	1230	46.60	CR	
G40W-B	150	300	33.1	314.0	52.00	1230	66.80	CR	
N-212-D1-A	140	190	32.1	226.2	63.44	1321	24.51	CR	[39]
N-212-D1-B	140	190	32.1	226.2	63.44	1321	23.85	CR	
N-216-D1-A	140	190	32.1	402.1	64.63	1015	29.82	CR	
N-216-D1-B	140	190	32.1	402.1	64.63	1015	29.79	CR	
N-316-D1-A	140	190	32.1	603.2	64.63	1015	31.49	CR	
N-316-D1-B	140	190	32.1	603.2	64.63	1015	33.13	CR	

Table A1. Cont.

Specimen	b_c (mm)	h_c (mm)	f_c (MPa)	A_f (mm ²)	E_f (GPa)	f_f (MPa)	M_{exp} (kNm)	Failure	Ref.
N-212-D2-A	160	190	32.1	226.2	63.44	1321	21.96	CR	
N-212-D2-B	160	190	32.1	226.2	63.44	1321	21.96	CR	
H-316-D1-A	140	190	54.5	603.2	64.63	1015	45.00	CR	
H-316-D1-B	140	190	54.5	603.2	64.63	1015	44.44	CR	
BG3	150	250	46.5	1140.1	42.00	670	88.21	CR	[35]
BC3	150	250	51.8	380.0	119.00	1475	93.57	CR	
SG3	500	120	45.9	1425.1	42.00	670	46.88	CR	
SC3	500	120	49.8	506.7	119.00	1475	52.50	CR	
BC2	150	250	52.6	214.0	132.00	1320	79.00	CR	
SG2	500	120	46.2	356.7	42.80	665	31.88	CR	
SC2	500	120	51.0	285.3	132.00	1320	42.38	CR	
BG2	150	250	47.7	253.4	41.60	620	61.36	CR	
S2-4-1nm	273	304	47.2	452.4	64.70	1468	87.50	CR	[82]
S2-4-2nm	276	303	49.4	452.4	64.70	1468	82.70	CR	
C-212-D1-a	140	190	59.8	226.2	63.25	1353	38.22	CR	[40]
C-212-D1-b	140	190	59.8	226.2	63.25	1353	35.58	CR	
C-216-D1-a	140	190	56.3	402.1	64.15	995	45.06	CR	
C-216-D1-b	140	190	56.3	402.1	64.15	995	43.02	CR	
C-316-D1-a	140	190	55.2	603.2	64.15	995	49.38	CR	
C-316-D1-b	140	190	55.2	603.2	64.15	995	50.94	CR	
C-212-D2-a	160	190	39.6	226.2	63.25	1353	27.69	CR	
C-212-D2-b	160	190	39.6	226.2	63.25	1353	25.53	CR	
C-216-D2-a	160	190	61.7	402.1	64.15	995	42.15	CR	
C-216-D2-b	160	190	61.7	402.1	64.15	995	40.47	CR	
C-316-D2-a	160	190	60.1	603.2	64.15	995	43.20	CR	
C-316-D2-b	160	190	60.1	603.2	64.15	995	47.16	CR	
BFRP1	80	140	32.8	150.8	39.05	1051.79	7.90	CR	[68]
BFRP2	80	140	32.8	150.8	39.05	1051.79	7.90	CR	
BFRP3	80	140	32.8	150.8	39.05	1051.79	7.50	CR	
SG-RGC-2-19	200	300	38.2	567.1	63.70	1105	91.40	CR	[58]
SG-RGC-3-15.9	200	300	38.2	595.7	62.60	1184	104.80	CR	
SG-RGC-4-12.7	200	300	38.2	506.7	65.60	1312	96.10	CR	
SG-RGC-5-15.9	200	300	38.2	992.8	62.60	1184	99.30	CR	
BFRP 5#9	200	300	52.3	293.8	56.30	1485	59.54	CR	[62]
BFRP 3#7	200	300	52.3	107.0	52.80	1185	28.76	FR	
B-4#10	200	300	42.5	316.0	44.40	1189	58.30	CR	[45]
B-4#12	200	300	42.5	452.0	45.30	1162	76.89	CR	
B-2#16	200	300	42.5	402.0	48.70	1173	69.74	CR	
B-4#16	200	300	42.5	804.0	48.70	1173	82.06	CR	
B-2#10	200	300	42.5	158.0	44.40	1189	52.84	CR	
B-2#12	200	300	42.5	226.0	45.30	1162	53.72	CR	
BRC20	200	300	47.2	628.3	46.20	907	75.78	CR	[83]
5#13G1	200	400	39.0	645.0	48.70	817	130.60	CR	[47]
2#13G2	200	400	33.5	258.0	67.00	1639	82.78	CR	
4#15G1	200	400	39.0	796.0	48.10	751	138.20	CR	
2#15G2	200	400	29.0	398.0	69.30	1362	95.93	CR	
2#15G3	200	400	33.8	398.0	59.50	1245	91.31	CR	
6#15G1	200	400	33.5	1194.0	48.10	751	118.30	CR	
5#15G2	200	400	29.0	995.0	69.30	1362	129.30	CR	
3#20G1	200	400	42.1	852.0	47.60	728	140.40	CR	
3#20G2	200	400	48.1	852.0	52.50	1082	171.40	CR	
2#25G2	200	400	48.1	1020.0	66.30	1132	167.20	CR	
2#25G3	200	400	33.8	1020.0	60.30	906	115.90	CR	
3#13G1	200	400	33.5	387.0	48.70	817	81.34	CR	
2#20G1	200	400	39.0	568.0	47.60	728	107.40	CR	
2#22G1	200	400	39.0	774.0	46.40	693	132.30	CR	
2#25G1	200	400	48.1	1020.0	53.20	666	161.70	CR	
2T10B	180	230	30.0	157.1	50.00	1190	23.44	CR	[31]
2T12B	180	230	30.0	226.2	50.00	1190	31.13	CR	
3T16B	180	230	30.0	603.2	50.00	1190	38.06	CR	

Table A1. Cont.

Specimen	b_c (mm)	h_c (mm)	f_c (MPa)	A_f (mm ²)	E_f (GPa)	f_f (MPa)	M_{exp} (kNm)	Failure	Ref.
B2-35-16	200	300	35.0	402.0	63.00	1122	72.90	CR	[29]
B3-35-20	200	300	35.0	628.0	69.00	1117	78.20	CR	
B4-35-25	200	300	35.0	980.0	65.00	1340	87.20	CR	
B6-65-16	200	300	65.0	402.0	63.00	1122	100.30	CR	
B7-65-20	200	300	65.0	628.0	69.00	1117	110.00	CR	[59]
B8-65-25	200	300	65.0	980.0	65.00	1340	124.10	CR	
B1-35-12	200	300	35.0	226.0	65.00	1166	50.90	CR	
B5-65-12	200	300	65.0	226.0	65.00	1166	73.50	FR	
2G_3G	200	300	31.0	593.7	62.60	1184	105.05	CR	[32]
2G_5G	200	300	31.0	989.5	62.60	1184	107.80	CR	
2S_3G	200	300	31.0	593.7	62.60	1184	98.70	CR	
C03-GPC20	110	300	20.0	84.0	148.00	2000	50.52	CR	
C06-GPC35	110	300	35.0	140.0	148.00	2000	57.00	CR	[43]
C09-GPC50	110	300	50.0	168.0	148.00	2000	67.92	CR	
C12-OPC35	110	300	35.0	140.0	148.00	2000	63.64	CR	
C05-GPC35	110	300	35.0	84.0	148.00	2000	54.16	CR	
C08-GPC50	110	300	50.0	112.0	148.00	2000	61.64	CR	[84]
C11-OPC35	110	300	35.0	84.0	148.00	2000	54.96	CR	
C01-GPC20	110	300	20.0	28.0	148.00	2000	20.96	FR	
C02-GPC20	110	300	20.0	56.0	148.00	2000	41.12	FR	
C04-GPC35	110	300	35.0	28.0	148.00	2000	22.28	FR	[65]
C07-GPC50	110	300	50.0	56.0	148.00	2000	45.00	FR	
C10-OPC35	110	300	35.0	28.0	148.00	2000	21.68	FR	
B10-0-0	120	240	38.5	157.0	47.60	1141	18.68	CR	
B13-0-0	120	240	38.5	265.0	48.60	1142	28.46	CR	[30]
GFRP-4S-13	100	200	39.6	265.5	43.00	673	18.00	CR	
GFRP-5S-13	100	200	39.6	265.5	43.00	673	20.25	CR	
GFRP-1S-10	100	200	39.6	157.1	43.00	673	11.93	CR	
GFRP-2S-10	100	200	39.6	157.1	43.00	673	13.05	CR	[53]
GFRP-3S-10	100	200	39.6	157.1	43.00	673	13.73	CR	
SA-B10-1	125	200	33.1	157.1	56.00	1565	14.95	CR	
SA-B10-2	125	200	33.1	157.1	56.00	1565	15.43	CR	
R-B10-1	125	200	35.5	157.1	54.00	1356	15.54	CR	[85]
R-B10-2	125	200	35.5	157.1	54.00	1356	15.50	CR	
2T12B-N	180	230	47.5	243.0	46.60	1118.6	31.10	CR	
3T16B-N	180	230	47.5	636.0	46.00	1121.3	38.30	CR	
2T12C-N	180	230	47.5	243.0	131.00	2068	41.60	CR	[86]
2T12B-H	180	230	70.5	243.0	46.60	1118.6	31.90	CR	
3T16B-H	180	230	70.5	636.0	46.00	1121.3	44.50	CR	
2T12C-H	180	230	70.5	243.0	131.00	2068	50.30	CR	
2T10B-N	180	230	47.5	171.0	42.80	1028.7	22.80	CR	[87]
3T8B-N	180	230	47.5	172.0	42.90	1075.1	23.00	CR	
3T8B-H	180	230	70.5	172.0	42.90	1075.1	26.00	CR	
2T10B-H	180	230	70.5	171.0	42.80	1028.7	24.80	CR	
OPC-S-FL-67	150	200	67.0	157.1	55.00	1200	25.29	CR	[87]
LG1-3	150	250	32.7	251.2	52.00	962	28.80	CR	
LG2-3	200	250	32.7	251.2	52.00	962	31.05	CR	
LG1-1	150	250	32.7	74.2	52.00	1200	15.00	CR	
LG2-2	200	250	32.7	143.6	52.00	1000	27.00	CR	[86]
LG1-2	150	250	32.7	143.6	52.00	1000	27.00	CR	
N-2#12-10-3.05	150	200	41.0	226.2	49.31	1075	24.47	CR	
N-4#12-10-3.13	150	200	41.0	452.4	49.31	1075	27.77	CR	
N-4#12-10-2.78	150	220	41.0	452.4	49.31	1075	32.56	CR	[87]
N-4#14-10-2.78	150	220	41.0	615.8	51.72	1102	36.25	CR	
N-5#12-10-2.51	150	250	41.0	565.5	49.31	1075	37.90	CR	
N-2#12-8-2.69	150	220	41.0	226.2	49.31	1075	25.36	FR	
N-2#14-8-2.70	150	220	41.0	307.9	51.72	1102	32.96	FR	[87]
N-2#12-8-2.43	150	250	41.0	226.2	49.31	1075	18.54	FR	
G2	150	200	35.0	402.1	52.54	958.41	23.39	CR	
G3	150	200	35.0	402.1	52.54	958.41	21.25	CR	

Table A1. Cont.

Specimen	b_c (mm)	h_c (mm)	f_c (MPa)	A_f (mm ²)	E_f (GPa)	f_f (MPa)	M_{exp} (kNm)	Failure	Ref.
G5	150	200	33.0	157.1	47.60	838.8933	14.90	CR	[60]
NB#16	200	300	34.4	452.9	49.20	988.5	61.10	CR	
NGII#12	200	300	34.4	294.8	48.30	980.2	52.10	CR	
NGIII#12	200	300	34.4	300.4	49.00	980.7	51.60	CR	
HB3#16	200	300	105.2	679.3	49.20	988.5	81.30	CR	
NB#10	200	300	34.4	166.3	43.90	1003.4	37.60	CR	
NB#12	200	300	34.4	267.5	45.70	983.5	53.20	CR	
NB3#10	200	300	34.4	249.5	43.90	1003.4	50.80	CR	
NGI#12	200	300	34.4	274.1	48.50	951.4	50.30	CR	
HB#16	200	300	105.2	452.9	49.20	988.5	87.80	FR	
C36G3Φ12	180	250	36.0	339.3	60.00	1000	43.96	CR	
C36G3Φ14	180	250	36.0	461.8	60.00	1000	54.50	CR	
C73G3Φ14	180	250	73.0	461.8	60.00	1000	63.11	CR	
C84G3Φ14	180	250	84.0	461.8	60.00	1000	70.00	CR	
C73G3Φ12	180	250	73.0	339.3	60.00	1000	58.98	CR	
C73G3Φ8	180	250	73.0	150.8	60.00	1000	27.37	FR	
C84G3Φ8	180	250	84.0	150.8	60.00	1000	29.96	FR	
C84G3Φ12	180	250	84.0	339.3	60.00	1000	56.11	FR	
C36G3Φ8	180	250	36.0	150.8	60.00	1000	28.46	FR	
2D16-8S70-N	250	250	30.0	402.0	46.00	775	50.80	CR	
2D16-10S110-N	250	250	30.0	402.0	46.00	775	52.80	CR	[56]
2D16-8S35-N	250	250	30.0	402.0	46.00	775	61.20	CR	
2D16-10S55-N	250	250	30.0	402.0	46.00	775	56.40	CR	
5D10-8S70-N	250	250	30.0	393.0	44.00	789	53.20	CR	
5D10-10S110-N	250	250	30.0	393.0	44.00	789	54.00	CR	
5D10-8S35-N	250	250	30.0	393.0	44.00	789	64.40	CR	
5D10-10S55-N	250	250	30.0	393.0	44.00	789	59.60	CR	
3D18-8S70-N	250	250	30.0	763.0	42.00	800	71.60	CR	
3D18-10S110-N	250	250	30.0	763.0	42.00	800	69.20	CR	
3D18-8S35-N	250	250	30.0	763.0	42.00	800	83.60	CR	
3D18-10S55-N	250	250	30.0	763.0	42.00	800	78.40	CR	
5D14-8S70-N	250	250	30.0	770.0	45.00	825	72.40	CR	
5D14-10S110-N	250	250	30.0	770.0	45.00	825	68.00	CR	
5D14-8S35-N	250	250	30.0	770.0	45.00	825	83.20	CR	
5D14-10S55-N	250	250	30.0	770.0	45.00	825	77.60	CR	
KD30-2	200	300	44.0	573.0	49.00	641	63.80	CR	
ISO30-2	200	300	44.0	573.0	42.00	689	80.40	CR	[41]
KD45-1	200	450	52.0	573.0	49.00	641	106.60	CR	
KD45-2	200	450	52.0	573.0	49.00	641	113.00	CR	
ISO55-1	200	550	43.0	573.0	42.00	689	181.50	FR	
ISO55-2	200	550	43.0	573.0	42.00	689	181.50	FR	
KD55-1	200	550	43.0	573.0	49.00	641	146.90	FR	
KD55-2	200	550	43.0	573.0	49.00	641	172.50	FR	
ISO2	200	300	43.0	573.0	45.00	600	80.40	CR	
ISO3	200	550	43.0	573.0	45.00	600	181.70	FR	
ISO4	200	550	43.0	573.0	45.00	600	181.70	FR	
U8-2.8	152	254	49.3	117.0	48.00	1150	25.32	CR	
U10-2.5	152	254	49.3	163.4	48.00	1150	37.40	CR	
U8-3.1	152	254	49.3	117.0	48.00	1150	26.18	FR	[55]
U8-2.5	152	254	49.3	117.0	48.00	1150	26.13	FR	
A2	152.4	304.8	29.0	213.0	49.64	896.32	37.62	CR	
AVH4	152.4	304.8	68.9	169.6	49.64	896.32	42.71	CR	
DH1	152.4	304.8	44.8	142.0	49.64	689.48	24.40	FR	[49]
DH6	152.4	304.8	44.8	142.0	49.64	689.48	22.40	FR	
DA	152.4	304.8	51.7	142.0	49.64	896.32	37.62	FR	
DB-ARCH	152.4	304.8	51.7	142.0	49.64	896.32	58.98	FR	
B3-I	150	300	66.3	226.2	42.50	746.54	34.45	CR	[87]
B3-II	150	300	114.9	226.2	42.50	746.54	53.95	CR	
B1-I	150	300	66.3	100.5	42.50	489.3	18.20	FR	
B2-I	150	300	66.3	157.1	42.50	637.02	23.08	FR	

Table A1. Cont.

Specimen	b_c (mm)	h_c (mm)	f_c (MPa)	A_f (mm ²)	E_f (GPa)	f_f (MPa)	M_{exp} (kNm)	Failure	Ref.
B2-II	150	300	114.9	157.1	42.50	637.02	39.65	FR	
Beam2	150	200	32.6	56.6	38.00	650	5.89	FR	[36]
Beam6	150	300	32.6	56.6	38.00	650	7.85	FR	
beam12	150	300	58.9	113.1	38.00	650	16.75	FR	
1	152	152	35.9	70.9	44.80	760	7.04	FR	[42]
2	152	152	35.9	70.9	44.80	760	6.64	FR	
4	152	152	35.9	70.9	44.80	760	7.23	FR	
5	152	152	35.9	70.9	44.80	760	7.35	FR	
6	152	152	35.9	70.9	44.80	760	6.75	FR	
C-C-3a	200	300	23.6	88.4	200.00	2000	44.76	FR	[37]
C-C-4a	200	300	27.2	226.2	200.00	1061	60.66	FR	
IS2B-1	200	293.5	42.7	299.1	45.00	552	38.50	FR	[50]
IS2B-2	200	293.5	54.4	299.1	45.00	552	41.00	FR	
KD2B-1	200	293.5	42.7	299.1	49.00	641	52.80	FR	
KD2B-2	200	293.5	42.7	449.2	49.00	641	61.60	FR	
Beam 2	100	175	102.0	603.2	50.49	520	36.30	FR	

Notes: CR is concrete crushing; FR is FRP rupture.

References

- Brandt, M.J.; Johnson, K.M.; Elphinston, A.J.; Ratnayaka, D.D. (Eds.) Chapter 5—Dams and reservoirs. In *Twort's Water Supply*, 7th ed.; Butterworth-Heinemann: Boston, MA, USA, 2017; pp. 159–204.
- Mir, M.A. Evolution of concrete skyscrapers: From ingalls to jin mao. *Electron. J. Struct. Eng.* **2001**, *1*, 2–14. [\[CrossRef\]](#)
- Chakraborty, S.; Mandal, R.; Chakraborty, S.; Guadagnini, M.; Pilakoutas, K. Chemical attack and corrosion resistance of concrete prepared with electrolyzed water. *J. Mater. Res. Technol.* **2021**, *11*, 1193–1205. [\[CrossRef\]](#)
- Al-Furjan, M.S.H.; Shan, L.; Shen, X.; Zarei, M.S.; Hajmohammad, M.H.; Kolahchi, R. A review on fabrication techniques and tensile properties of glass, carbon, and kevlar fiber reinforced rolymer composites. *J. Mater. Res. Technol.* **2022**, *19*, 2930–2959. [\[CrossRef\]](#)
- Bakis, C.E.; Bank Lawrence, C.; Brown, V.L.; Cosenza, E.; Davalos, J.F.; Lesko, J.J.; Machida, A.; Rizkalla, S.H.; Triantafillou, T.C. Fiber-reinforced polymer composites for construction—State-of-the-art review. *J. Compos. Constr.* **2002**, *6*, 73–87. [\[CrossRef\]](#)
- Zhang, R.; Li, Z.; Sun, Q.; Yu, G.; Wang, X.; Wu, L. Design and characterization of the carbon fiber tube reinforced polymer composite for full ocean depth submersibles. *Compos. Sci. Technol.* **2022**, *217*, 109074. [\[CrossRef\]](#)
- Rosa, I.; Firmo, J.; Correia, J.; Mazzuca, P. Influence of Elevated Temperatures on the Bond Behaviour of Gfrp Bars to Concrete—Pull-Out Tests. In Proceedings of the IABSE Symposium 2019 Guimaraes: Towards a Resilient Built Environment-Risk and Asset Management, Guimaraes, Portugal, 27–29 March 2019; International Association for Bridge and Structural Engineering (IABSE): Zurich, Switzerland, 2019; pp. 861–868.
- Rosa, I.C.; Firmo, J.P.; Correia, J.R.; Mazzuca, P. Influence of elevated temperatures on the bond behaviour of ribbed gfrp bars in concrete. *Cem. Concr. Compos.* **2021**, *122*, 104119. [\[CrossRef\]](#)
- Rosa Inês, C.; Firmo João, P.; Correia João, R.; Bisby Luke, A. Fire behavior of gfrp-reinforced concrete structural members: A state-of-the-art review. *J. Compos. Constr.* **2023**, *27*, 03123002. [\[CrossRef\]](#)
- Clark, J.C.; Davids, W.G.; Lopez-Anido, R.A.; Schanck, A.P.; Sheltra, C.A. Continuously formed fiber-reinforced thermoplastic composite rebar for concrete reinforcement. *J. Compos. Sci.* **2025**, *9*, 378. [\[CrossRef\]](#)
- Di, B.; Qin, R.; Zheng, Y.; Lv, J. Investigation of the shear behavior of concrete beams reinforced with frp rebars and stirrups using ann hybridized with genetic algorithm. *Polymers* **2023**, *15*, 2857. [\[CrossRef\]](#) [\[PubMed\]](#)
- Duarte, I.O.; Forti, N.C.; Pimentel, L.L.; Jacintho, A.E. A study of the shear behavior of concrete beams with synthetic fibers reinforced with glass and basalt fiber-reinforced polymer bars. *Buildings* **2024**, *14*, 2123. [\[CrossRef\]](#)
- Feng, L.; Li, P.-D.; Huang, X.-X.; Wu, Y.-F. Reliability-based design analysis for frp reinforced compression yield beams. *Polymers* **2022**, *14*, 4846. [\[CrossRef\]](#)
- Ge, W.; Zhang, F.; Sushant, S.; Yao, S.; Ashour, A.; Luo, L.; Jiang, H.; Zhang, Z. Parametric analysis on flexural performance of reactive powder concrete frame beams reinforced with steel-frp composite bars. *Structures* **2024**, *60*, 105942. [\[CrossRef\]](#)
- Goonewardena, J.; Ghabraie, K.; Subhani, M. Flexural performance of frp-reinforced geopolymer concrete beam. *J. Compos. Sci.* **2020**, *4*, 187. [\[CrossRef\]](#)
- Ramamoorthy, D.; Guo, B.; Kazmi, S.M.; Wu, Y. A reliability-based design approach for the flexural resistance of compression yielded fibre-reinforced polymer (frp)-reinforced concrete beams. *Buildings* **2024**, *14*, 2415. [\[CrossRef\]](#)

17. Tran, H.; Nguyen-Thoi, T.; Dinh, H.-B. State-of-the-art review of studies on the flexural behavior and design of frp-reinforced concrete beams. *Materials* **2025**, *18*, 3295. [CrossRef] [PubMed]
18. Zhao, J.; Pan, H.; Wang, Z.; Li, G. Experimental and theoretical study on flexural behavior of gfrp- and cfrp-reinforced concrete beams after high-temperature exposure. *Polymers* **2022**, *14*, 4002. [CrossRef] [PubMed]
19. Zhao, J.; Zhu, M.; Xu, L.; Chen, M.; Shi, M. Prediction of shear capacity of fiber-reinforced polymer-reinforced concrete beams based on machine learning. *Buildings* **2025**, *15*, 1908. [CrossRef]
20. Selcuk, S.; Ahmetoglu, U.; Gokce, E.C. Basalt fiber reinforced polymer composites (bfrp) other than rebars: A review. *Mater. Today Commun.* **2023**, *37*, 107359. [CrossRef]
21. ACI 440.1R-15; Guide for the Design and Construction of Structural Concrete Reinforced with Fiber—Reinforced Polymer (Frp) Bars. American Concrete Institute: Farmington Hills, MI, USA, 2015.
22. CSA-S806-02; Design and Construction of Building Components with Fiber-Reinforced Polymers. Canadian Standards Association: Toronto, ON, Canada, 2007.
23. CEB-FIB. *Frp Reinforcement in Rc Structures*; FIB International: Lausanne, Switzerland, 2007.
24. Masoud Hassanzadeh, A.; Dehestani, M.; Nazarpour, H. Reliability analysis of flexural provisions of frp-rc beams and sensitivity analysis based on form. *Eng. Struct.* **2023**, *285*, 116037. [CrossRef]
25. Behnam, B.; Eamon, C. Reliability-based design optimization of concrete flexural members reinforced with ductile frp bars. *Constr. Build. Mater.* **2013**, *47*, 942–950. [CrossRef]
26. He, Z.; Qiu, F. Probabilistic assessment on flexural capacity of gfrp-reinforced concrete beams designed by guideline aci 440.1r-06. *Constr. Build. Mater.* **2011**, *25*, 1663–1670. [CrossRef]
27. Ribeiro, S.E.C.; Diniz, S.M.C. Reliability-based design recommendations for frp-reinforced concrete beams. *Eng. Struct.* **2013**, *52*, 273–283. [CrossRef]
28. Eurocode-2. Design of Concrete Structures—Part 1-1: General Rules and Rules for Buildings. The European Union per Regulation 305/2011: 2004. Available online: <https://www.phd.eng.br/wp-content/uploads/2015/12/en.1992.1.1.2004.pdf> (accessed on 5 March 2024).
29. Abdelkarim, O.I.; Ahmed, E.A.; Mohamed, H.M.; Benmokrane, B. Flexural strength and serviceability evaluation of concrete beams reinforced with deformed gfrp bars. *Eng. Struct.* **2019**, *186*, 282–296. [CrossRef]
30. Abed, F.; Al-Mimar, M.; Ahmed, S. Performance of bfrp rc beams using high strength concrete. *Compos. Part C Open Access* **2021**, *4*, 100107. [CrossRef]
31. Abed, F.; Al-Mimar, M.; Tello, N. Evaluation of bfrp rc Beams Under Flexure. In Proceedings of the 2019 Advances in Science and Engineering Technology International Conferences (ASET), Dubai, United Arab Emirates, 26 March–10 April 2019; IEEE: New York, NY, USA, 2019; pp. 1–4.
32. Ahmed, H.Q.; Jaf, D.K.; Yaseen, S.A. Flexural strength and failure of geopolymer concrete beams reinforced with carbon fibre-reinforced polymer bars. *Constr. Build. Mater.* **2020**, *231*, 117185. [CrossRef]
33. Almusallam, T.H.; Al-Salloum, Y.A.; Alsayed, S.H.; Amjad, M.A. Behavior of Concrete Beams Doubly Reinforced by Frp Bars. In Proceedings of the Third International Symposium on Non-Metallic (FRP) Reinforcement for Concrete Structures (FRPRCS-3), Sapporo, Japan, 14–16 October 1997; pp. 471–478.
34. Alsayed, S.H.; Al-Salloum, Y.A.; Almusallam, T.H. Performance of glass fiber reinforced plastic bars as a reinforcing material for concrete structures. *Compos. Part B Eng.* **2000**, *31*, 555–567. [CrossRef]
35. Al-Sunna, R.; Pilakoutas, K.; Hajirasouliha, I.; Guadagnini, M. Deflection behaviour of frp reinforced concrete beams and slabs: An experimental investigation. *Compos. Part B Eng.* **2012**, *43*, 2125–2134. [CrossRef]
36. Ashour, A.F. Flexural and shear capacities of concrete beams reinforced with gfrp bars. *Constr. Build. Mater.* **2006**, *20*, 1005–1015. [CrossRef]
37. Ashour, A.F.; Habeeb, M.N. Continuous concrete beams reinforced with cfrp bars. *Proc. Inst. Civ. Eng. Struct. Build.* **2008**, *161*, 349–357. [CrossRef]
38. Benmokrane, B.; Chaallal, O.; Masmoudi, R. Flexural response of concrete beams reinforced with frp reinforcing bars. *Struct. J.* **1996**, *93*, 46–55.
39. Barris, C.; Torres, L.; Comas, J.; Miàs, C. Cracking and deflections in gfrp rc beams: An experimental study. *Compos. Part B Eng.* **2013**, *55*, 580–590. [CrossRef]
40. Barris, C.; Torres, L.; Turon, A.; Baena, M.; Catalan, A. An experimental study of the flexural behaviour of gfrp rc beams and comparison with prediction models. *Compos. Struct.* **2009**, *91*, 286–295. [CrossRef]
41. Benmokrane, B.; Chaallal, O.; Masmoudi, R. Glass fibre reinforced plastic (gfrp) rebars for concrete structures. *Constr. Build. Mater.* **1995**, *9*, 353–364. [CrossRef]
42. Brown, V.L.; Bartholomew, C.L. Frp reinforcing bars in reinforced concrete members. *Mater. J.* **1993**, *90*, 34–39.
43. Dong, Z.; Wu, G.; Zhu, H.; Zhao, X.-L.; Wei, Y.; Qian, H. Flexural behavior of seawater sea-sand coral concrete–uhpc composite beams reinforced with bfrp bars. *Constr. Build. Mater.* **2020**, *265*, 120279. [CrossRef]

44. Duranovic, N.; Pilakoutas, K.; Waldron, P. Tests on Concrete Beams Reinforced with Glass Fibre Reinforced Plastic Bars. In Proceedings of the Third International Symposium on Non-Metallic (FRP) Reinforcement for Concrete Structures (FRPRCS-3), Sapporo, Japan, 14–16 October 1997; pp. 479–486.
45. Elgabbas, F.; Vincent, P.; Ahmed, E.A.; Benmokrane, B. Experimental testing of basalt-fiber-reinforced polymer bars in concrete beams. *Compos. Part B Eng.* **2016**, *91*, 205–218. [\[CrossRef\]](#)
46. El-Nemr, A.; Ahmed, E.A.; Benmokrane, B. Flexural behavior and serviceability of normal-and high-strength concrete beams reinforced with glass fiber-reinforced polymer bars. *ACI Struct. J.* **2013**, *110*, 1077–1088.
47. El-Nemr, A.; Ahmed, E.A.; El-Safty, A.; Benmokrane, B. Evaluation of the flexural strength and serviceability of concrete beams reinforced with different types of gfrp bars. *Eng. Struct.* **2018**, *173*, 606–619. [\[CrossRef\]](#)
48. Escórcio, P.; França, P.M. Experimental study of a rehabilitation solution that uses gfrp bars to replace the steel bars of reinforced concrete beams. *Eng. Struct.* **2016**, *128*, 166–183. [\[CrossRef\]](#)
49. Faza, S.S. Bending and Bond Behavior and Design of Concrete Beams Reinforced with Fiber-Reinforced Plastic Rebars. Ph.D. Thesis, West Virginia University, Morgantown, WV, USA, 1991.
50. Gao, D.; Benmokrane, B. Calculation method of flexural capacity of gfrp-reinforced concrete beam. *J. Hydraul. Eng.* **2001**, *4*, 73–80.
51. He, Z.; Ou, J.; Wang, B. The trilinear moment vs. Curvature relationship of concrete beams reinforced with fiber reinforced polymer (frp) rebars. *Compos. Struct.* **2007**, *77*, 30–35. [\[CrossRef\]](#)
52. Houssam, A.T.; Mohamed, S. Flexural behavior of concrete beams reinforced with glass fiber-reinforced polymer (gfrp) bars. *Struct. J.* **2000**, *97*, 712–719.
53. Huang, Z.; Chen, W.; Tran, T.T.; Pham, T.M.; Hao, H.; Chen, Z.; Elchalakani, M. Experimental and numerical study on concrete beams reinforced with basalt frp bars under static and impact loads. *Compos. Struct.* **2021**, *263*, 113648. [\[CrossRef\]](#)
54. Kassem, C.; Farghaly Ahmed, S.; Benmokrane, B. Evaluation of flexural behavior and serviceability performance of concrete beams reinforced with frp bars. *J. Compos. Constr.* **2011**, *15*, 682–695. [\[CrossRef\]](#)
55. Khanfour, M.-A.; El Refai, A. Effect of freeze-thaw cycles on concrete reinforced with basalt-fiber reinforced polymers (bfrp) bars. *Constr. Build. Mater.* **2017**, *145*, 135–146. [\[CrossRef\]](#)
56. Khorasani, A.M.M.; Esfahani, M.R.; Sabzi, J. The effect of transverse and flexural reinforcement on deflection and cracking of gfrp bar reinforced concrete beams. *Compos. Part B Eng.* **2019**, *161*, 530–546. [\[CrossRef\]](#)
57. Lau, D.; Pam, H.J. Experimental study of hybrid frp reinforced concrete beams. *Eng. Struct.* **2010**, *32*, 3857–3865. [\[CrossRef\]](#)
58. Maranan, G.B.; Manalo, A.C.; Benmokrane, B.; Karunasena, W.; Mendis, P. Evaluation of the flexural strength and serviceability of geopolymer concrete beams reinforced with glass-fibre-reinforced polymer (gfrp) bars. *Eng. Struct.* **2015**, *101*, 529–541. [\[CrossRef\]](#)
59. Maranan, G.B.; Manalo, A.C.; Benmokrane, B.; Karunasena, W.; Mendis, P.; Nguyen, T.Q. Flexural behavior of geopolymer-concrete beams longitudinally reinforced with gfrp and steel hybrid reinforcements. *Eng. Struct.* **2019**, *182*, 141–152. [\[CrossRef\]](#)
60. Mostafa, O.M.; Rahman, M.K.; Al-Zahrani, M.M.; Adekunle, S.K.; Al-Osta, M.A.; Najamuddin, S.K. Flexural behavior and bond coefficient of bfrp bar reinforced normal and high strength concrete beams. *Constr. Build. Mater.* **2023**, *401*, 132896. [\[CrossRef\]](#)
61. Muhammad, M.A.; Ahmed, F.R. Evaluation of deflection and flexural performance of reinforced concrete beams with glass fiber reinforced polymer bars. *Case Stud. Constr. Mater.* **2023**, *18*, e01855. [\[CrossRef\]](#)
62. Pawłowski, D.; Szumigala, M. Flexural behaviour of full-scale basalt frp rc beams—Experimental and numerical studies. *Procedia Eng.* **2015**, *108*, 518–525. [\[CrossRef\]](#)
63. Radhouane Masmoudi, M.T.; Brahim, B. Flexural behavior of concrete beams reinforced with deformed fiber reinforced plastic reinforcing rods. *Struct. J.* **1998**, *95*, 665–676.
64. San-José, J.T.; Vegas, I.; Meyer, F. Structural analysis of frp reinforced polymer concrete material. *Constr. Build. Mater.* **2006**, *20*, 971–981. [\[CrossRef\]](#)
65. Shamass, R.; Cashell, K.A. Experimental investigation into the flexural behaviour of basalt frp reinforced concrete members. *Eng. Struct.* **2020**, *220*, 110950. [\[CrossRef\]](#)
66. Thériault, M.; Benmokrane, B. Effects of frp reinforcement ratio and concrete strength on flexural behavior of concrete beams. *J. Compos. Constr.* **1998**, *2*, 7–16. [\[CrossRef\]](#)
67. Thiagarajan, G. Experimental and analytical behavior of carbon fiber-based rods as flexural reinforcement. *J. Compos. Constr.* **2003**, *7*, 64–72. [\[CrossRef\]](#)
68. Urbanski, M.; Lapko, A.; Garbacz, A. Investigation on concrete beams reinforced with basalt rebars as an effective alternative of conventional r/c structures. *Procedia Eng.* **2013**, *57*, 1183–1191. [\[CrossRef\]](#)
69. Stephens, M.A. Edf statistics for goodness of fit and some comparisons. *J. Am. Stat. Assoc.* **1974**, *69*, 730–737. [\[CrossRef\]](#)
70. Shayan, S. System Reliability-Based Design of 2d Steel Frames by Advanced Analysis. Ph.D. Thesis, The University of Sydney, Sydney, Australia, 2013.
71. Andrzej, S.N.; Maria, M.S. Calibration of design code for buildings (aci 318): Part 1—Statistical models for resistance. *Struct. J.* **2003**, *100*, 377–382.
72. Fishman, G. *Monte Carlo: Concepts, Algorithms, and Applications*; Springer Science & Business Media: Berlin/Heidelberg, Germany, 2013.

73. Au, S.-K.; Beck, J.L. Estimation of small failure probabilities in high dimensions by subset simulation. *Probabilistic Eng. Mech.* **2001**, *16*, 263–277. [[CrossRef](#)]
74. Huang, X.; Sui, L.; Xing, F.; Zhou, Y.; Wu, Y. Reliability assessment for flexural frp-strengthened reinforced concrete beams based on importance sampling. *Compos. Part B Eng.* **2019**, *156*, 378–398. [[CrossRef](#)]
75. Iervolino, I.; Galasso, C. Comparative assessment of load–resistance factor design of frp-reinforced cross sections. *Constr. Build. Mater.* **2012**, *34*, 151–161. [[CrossRef](#)]
76. Lu, R.; Luo, Y.; Conte, J.P. Reliability evaluation of reinforced concrete beams. *Struct. Saf.* **1994**, *14*, 277–298. [[CrossRef](#)]
77. Galambos Theodore, V.; Ellingwood, B.; MacGregor James, G.; Cornell, C.A. Probability based load criteria: Assessment of current design practice. *J. Struct. Div.* **1982**, *108*, 959–977. [[CrossRef](#)]
78. JCSS. Probabilistic Model Code. 2000. Available online: <https://www.jcss-lc.org/jcss-probabilistic-model-code> (accessed on 5 March 2024).
79. Yost Joseph, R.; Goodspeed Charles, H.; Schmeckpeper Edwin, R. Flexural performance of concrete beams reinforced with frp grids. *J. Compos. Constr.* **2001**, *5*, 18–25. [[CrossRef](#)]
80. Wang, H.; Belarbi, A. Flexural behavior of fiber-reinforced-concrete beams reinforced with frp rebars. *ACI Struct. J.* **2005**, *51*, 895–914.
81. Mahroug, M.E.M.; Ashour, A.F.; Lam, D. Tests of continuous concrete slabs reinforced with carbon fibre reinforced polymer bars. *Compos. Part B Eng.* **2014**, *66*, 348–357. [[CrossRef](#)]
82. Gribniak, V.; Kaklauskas, G.; Torres, L.; Daniunas, A.; Timinskas, E.; Gudonis, E. Comparative analysis of deformations and tension-stiffening in concrete beams reinforced with gfrp or steel bars and fibers. *Compos. Part B Eng.* **2013**, *50*, 158–170. [[CrossRef](#)]
83. Yuan, F.; Pan, J.; Leung, C.K.Y. Flexural behaviors of ecc and concrete/ecc composite beams reinforced with basalt fiber-reinforced polymer. *J. Compos. Constr.* **2013**, *17*, 591–602. [[CrossRef](#)]
84. Ramachandra Murthy, A.; Pukazhendhi, D.M.; Vishnuvardhan, S.; Saravanan, M.; Gandhi, P. Performance of concrete beams reinforced with gfrp bars under monotonic loading. *Structures* **2020**, *27*, 1274–1288. [[CrossRef](#)]
85. Zhang, X. Research on Short-Term Bending Stiffness and Deformation Behavior of Gfrp Reinforced Concrete Beams. Ph.D. Thesis, Harbin Institute of Technology, Harbin, China, 2015.
86. Wang, Z.; Xie, J.; Li, J.; Liu, P.; Shi, C.; Lu, Z. Flexural behaviour of seawater–sea sand concrete beams reinforced with gfrp bars: Effects of the reinforcement ratio, stirrup ratio, shear span ratio and prestress level. *J. Build. Eng.* **2022**, *54*, 104566. [[CrossRef](#)]
87. Ifrahim, M.S.; Sangi, A.J.; Ahmad, S.H. Experimental and numerical investigation of flexural behaviour of concrete beams reinforced with gfrp bars. *Structures* **2023**, *56*, 104951. [[CrossRef](#)]

Disclaimer/Publisher’s Note: The statements, opinions and data contained in all publications are solely those of the individual author(s) and contributor(s) and not of MDPI and/or the editor(s). MDPI and/or the editor(s) disclaim responsibility for any injury to people or property resulting from any ideas, methods, instructions or products referred to in the content.